Report No. ACNP-62001

PATHFINDER ATOMIC POWER PLANT

ANALOG SIMULATOR

Submitted to

U. S. ATOMIC ENERGY COMMISSION

NORTHERN STATES POWER COMPANY

and

CENTRAL UTILITIES ATOMIC POWER ASSOCIATES

by

ALLIS-CHALMERS MANUFACTURING COMPANY
ATOMIC ENERGY DIVISION
Milwaukee 1, Wisconsin

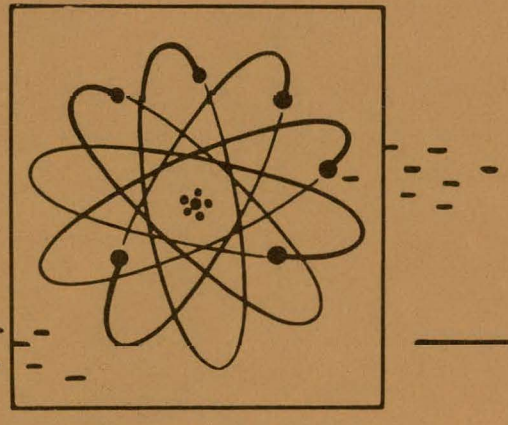

Ref: AEC Contract No. AT(11-1)-589

DISCLAIMER

LEGAL NOTICE

This report was prepared as an account of Government sponsored work. Neither the United States, nor the Commission, nor Allis-Chalmers Manufacturing Company, nor any person acting on behalf of the Commission or Allis-Chalmers Manufacturing Company:

A. Makes any warranty or representation to others, expressed or implied, with respect to the accuracy, completeness, or usefulness of the information contained in this report, or that the use of any information, apparatus, method, or process disclosed in this report may not infringe privately owned rights; or

B. Assumes any liabilities to others with respect to the use of, or for damages resulting from the use of any information, apparatus, method, or process disclosed in this report.

As used in the above, 'person acting on behalf of the Commission or Allis-Chalmers Manufacturing Company' includes any employe or contractor of the Commission, or Allis-Chalmers Manufacturing Company or employe of such contractor, to the extent that such employe or contractor of the Commission, or Allis-Chalmers Manufacturing Company or employe of such contractor prepares, disseminates, or provides access to, any information pursuant to his employment or contract with the Commission or Allis-Chalmers Manufacturing Company or his employment with such contractor.

PATHFINDER ATOMIC POWER PLANT
ANALOG SIMULATOR

by
D. H. Crimmins, D. Mohr and J. T. Stone

Submitted to

U. S. ATOMIC ENERGY COMMISSION
NORTHERN STATES POWER COMPANY
and
CENTRAL UTILITIES ATOMIC POWER ASSOCIATES

by

ALLIS-CHALMERS MANUFACTURING COMPANY

Under
Agreement dated 2nd Day of May 1957, as Amended
between
Allis-Chalmers Mfg. Co. & Northern States Power Co.
under
AEC Contract No. AT(11-1)-589

January 31, 1962

Classification – UNCLASSIFIED

Reviewed by R. G. Michel

Authorized Classifying Official

Approved: W. M. Hawkins
W. M. Hawkins
Mgr., Research and Development
Nuclear Power Dept.-Greendale

Approved: C. B. Graham
C. B. Graham
Manager
Nuclear Power Dept.-Greendale

ALLIS-CHALMERS MANUFACTURING COMPANY
ATOMIC ENERGY DIVISION
MILWAUKEE 1, WISCONSIN

Approved: Hibbert Hill
Hibbert Hill
Chief Engineer

NORTHERN STATES POWER COMPANY
15 SOUTH FIFTH STREET
MINNEAPOLIS 2, MINNESOTA

PATHFINDER ATOMIC POWER PLANT

ANALOG SIMULATOR

Distribution

USAEC, Chicago Operations Office - 9800 South Cass Avenue, Argonne, Illinois		8
USAEC, Division of Reactor Development - Washington 25, D. C.		8
USAEC, OTIE - Oak Ridge, Tennessee	OFFSET MASTER plus	20
Northern States Power Company and CUAPA		35
Allis-Chalmers Manufacturing Company		39
		110

FOREWORD

This topical report, one of a series on research and development for the Pathfinder Atomic Power Plant, is the final report on the Pathfinder transient simulator and the assumptions used in its derivations. An interim report on this same subject was issued as the first section of Allis-Chalmers Report No. ACNP-6005, entitled "Pathfinder Atomic Power Plant, Interim Progress Report of Reactor System Dynamic Analysis with Pathfinder Transient Simulator". Problems that have been solved with the transient simulator will be included in a subsequent report.

The Pathfinder Atomic Power Plant, which will be located at a site near Sioux Falls, South Dakota, is scheduled for operation in June 1962. Owners and operators of the plant will be the Northern States Power Company of Minneapolis, Minnesota. Allis-Chalmers Manufacturing Company of Milwaukee, Wisconsin, under contract with Northern States Power Company, the U.S. Atomic Energy Commission, and Central Utilities Atomic Power Associates (CUAPA), is performing the research, development, and design, and is responsible for construction of the plant. Conceptual engineering and component research and development is being done at Allis-Chalmers Greendale Laboratories.

CUAPA member companies are as follows: Central Electric and Gas Company; Interstate Power Company; Iowa Power and Light Company; Iowa Southern Utilities Company; Madison Gas and Electric Company; Northern States Power Company; Northwestern Public Service Company; Otter-Tail Power Company; St. Joseph Light and Power Company; and Wisconsin Public Service Corporation.

ACKNOWLEDGMENT

The authors wish to acknowledge Robert Mudd and Wen King for help in the design and operation of circuits shown in Section 15.

ABSTRACT

The steady-state and dynamic characteristics of the Pathfinder systems have been simulated on a dual-console Pace Analog Computer. The derivation of the system equations, the assumptions involved, their numerical evaluation, and their conversion to analog circuitry are described in this report.

The Pathfinder system is unique because of the internal nuclear superheater, and controlled, forced recirculation. In simulating this system the following major assumptions were made. The reactor is a boiling-water type; moderated and cooled with saturated, light water; pressurized between 400 and 800 psia; and has a neutron flux distribution that is spatially invariant. All the important non-linearities are retained, thus permitting accurate solutions of large system disturbances.

The neutron kinetics equations, with their six groups of delayed neutrons, are simulated with power feedbacks through reactor pressure, steam flow, core inlet subcooling, and fuel-element temperature. Particular attention is devoted to the accurate simulation of fuel-element heat transfer; the reactor pressure-control system, which operates the turbine inlet valves; and the effect of core inlet subcooling, since these were found to have pronounced effects on reactor performance. The transient temperatures at the superheater hot spot and exit are generated. Enough flexibility is included, so that all important disturbances possible in the actual plant can be run on the simulator. Changes in system parameters are easily accomplished by merely changing potentiometer settings.

The prime objectives of the reactor simulator are 1) to establish a control system for Pathfinder and optimize its settings, 2) to investigate system stability under all conditions, 3) to compute results of postulated system disturbances and accidents, and 4) to help obtain system characteristics useful in formulating plant operating procedures.

THIS PAGE

WAS INTENTIONALLY

LEFT BLANK

CONTENTS

ILLUSTRATIONS

ILLUSTRATIONS (Cont.)

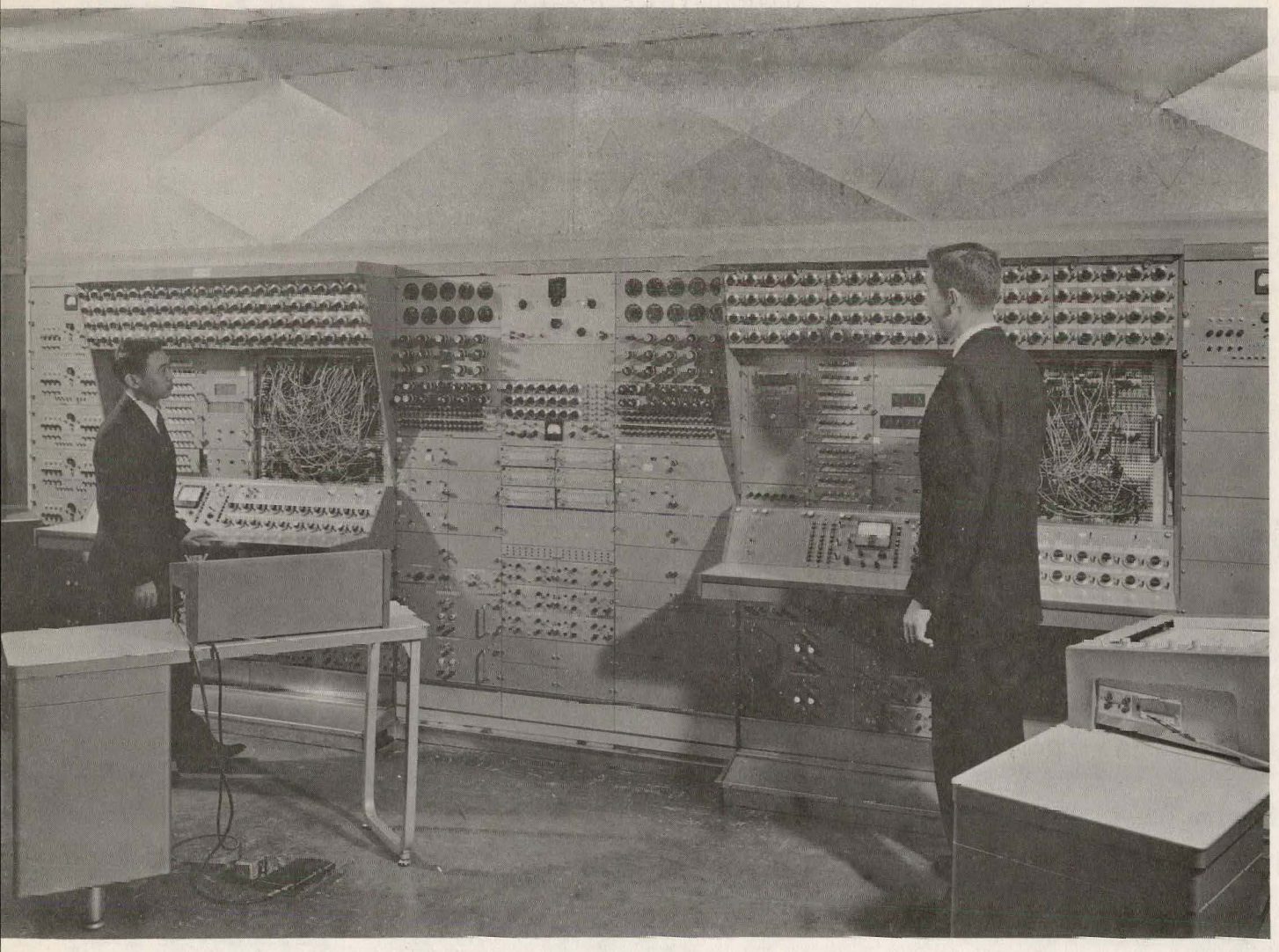

Analog Simulator (AC Photo 215540)

INTRODUCTION

In order to provide adequate control systems and operating procedures, and to insure safe, stable, and reliable operation of the Pathfinder Atomic Power Plant, a detailed knowledge of operating characteristics of the reactor and plant is required. To provide this knowledge, a transient simulator was constructed. All the pertinent reactor and system equations are derived and simulated on an Electronic Associates Analog Computer (Pace 231-R). The result is a coherent simulation of the Pathfinder Plant which is designated the Pathfinder Transient Simulator.

The simulator has been used to:

1. Help design and analyze reactor system controls.

2. Compute results of postulated operational disturbances, accidents, and operating errors.

3. Help establish operating and startup-shutdown procedures.

4. Predict system stability.

5. Show the effects of varying such parameters as power, pressure, void coefficients, and controller constants on transient response.

6. Help train Pathfinder reactor operators.

The Pathfinder Plant is moderated and cooled by light water. The core consists of two regions: an annular boiler region in which saturated steam is produced, and a central superheater region in which steam is superheated. Superheated steam passes directly to the turbine.

Among the advanced features that are incorporated in the plant in addition to the integral superheater, is the forced recirculation system. The recirculation

system includes three externally located centrifugal pumps. Recirculation flow rate is adjusted by means of the butterfly valves on the discharge side of the recirculation pumps.

Pressure in the main steam line is regulated automatically by positioning the turbine inlet valves. Thus, no steam is bypassed during normal operation and the electrical system absorbs normal changes in reactor output. A signal transmitting changes in superheater-exit steam temperature is also fed into this control system to modify the pressure set-point. This serves to minimize superheater temperature transients.

I. GENERAL DESCRIPTION OF SIMULATOR

The integro-differential equations are derived to describe the transient performance of the Pathfinder reactor and associated system. In deriving the equations, it is assumed that the reactor is:

1. Moderated and cooled by saturated light water.
2. Pressurized between 400 psia and 800 psia.
3. Assumed to be a point reactor, i.e. only the time variation of the neutron population is considered, not the distribution of the neutron population.

A simplified block diagram of the simulator is shown in Figure I.1. The "Reactor Kinetics" block represents the neutron kinetics equations and six delayed neutron groups. The average neutron population is simulated since a point reactor is assumed. Because of the close nuclear coupling of the Pathfinder core, it is also assumed that the superheater-region neutron kinetics are identical to the boiler-region neutron kinetics with negligible reactivity feedback from the superheater section.

The "Boiler Heat Transfer" block represents, with a distributed-parameter model, the time lag between heat generation in the cylindrical ceramic fuel pins

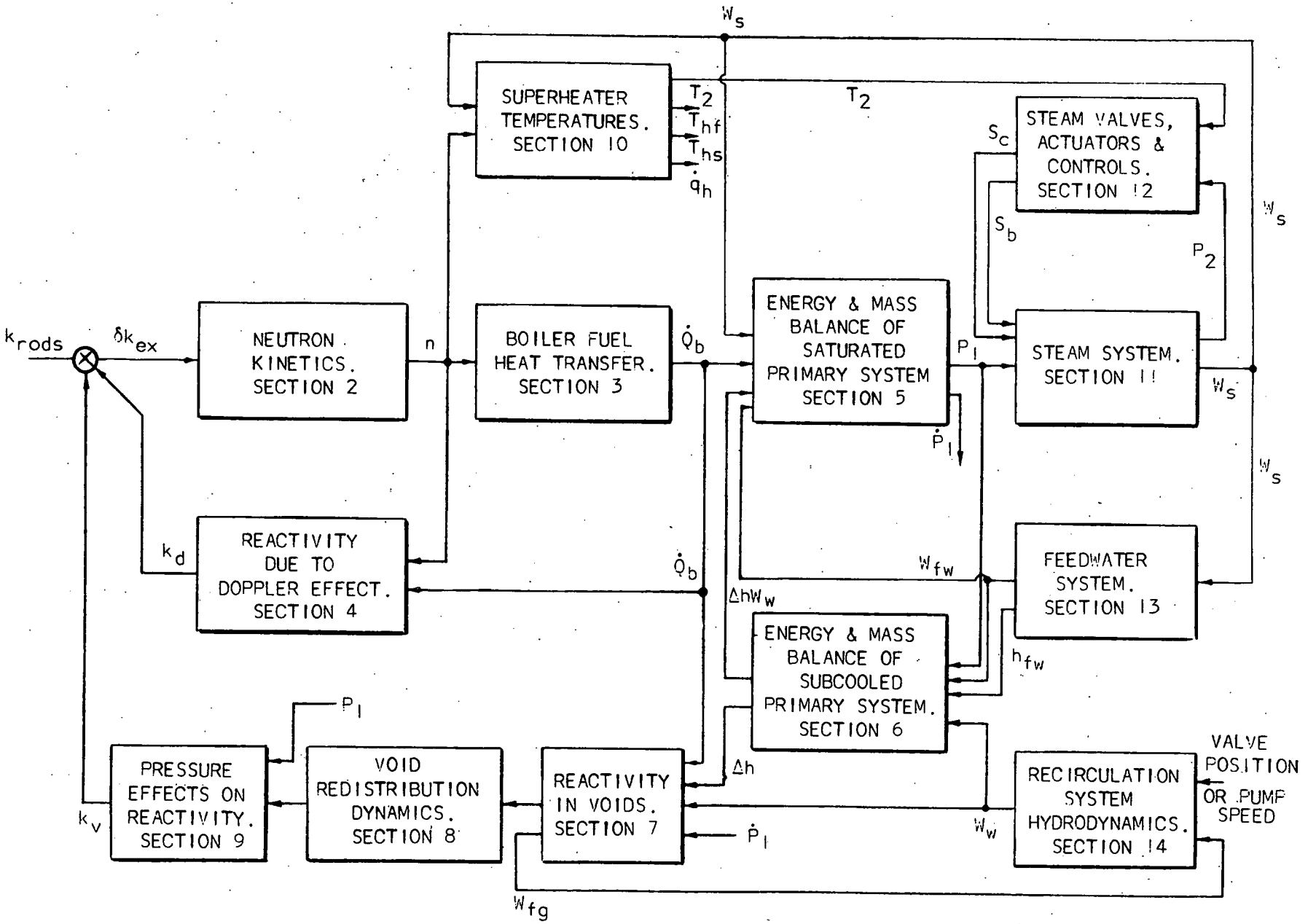

Figure 1.1 Simplified block diagram of Pathfinder Transient Simulator.
(A-C Dwg. 43-024-709)

and the heat flow into the coolant. The thermal resistance includes an appropriate average film heat-transfer coefficient for flowing boiling water at 615 psia.

"Reactivity due to Doppler effect" is the effect of boiler fuel temperature on core reactivity due to a shift in the neutron energy spectrum.

The "Energy and Mass Balance of Saturated Primary System" calculates the rate of pressure change due to an unbalance in the summation of energy terms associated with the boiler heat flux, steam leaving the vessel, and water entering the core. The energy of the water entering the core is found from a similar balance of the subcooled part of the primary system, including the transport time through the recirculation loop.

The reactivity held in voids ("Reactivity in Voids") depends on the core power, inlet subcooling, and recirculation flow rate. It is also affected by reactor pressure because of density changes and transient flashing and condensation of the steam.

The "Void Redistribution Dynamics" accounts for the time lag involved in changing void reactivity due to void redistribution. This lag is associated with the boiler-core steam transport time.

With steam flow and neutron flux as the inputs, the "Superheater Temperatures" block describes the transient temperatures of the superheater exit steam, the fuel hot spot, and the steam at the hot spot. The heat transfer coefficient varies with steam flow, and conservative hot-spot factors are used.

The "Steam System", "Steam Valve Actuators and Controls", and "Feedwater System" describe the superheater pressure drop and all components external to the

reactor vessel including the steam piping and turbine flow characteristics, turbine inlet valve and dump valve controls (under both normal and emergency conditions), feedwater temperature, and flow regulators, safety valves, etc.

The "Recirculation System Hydrodynamics" considers the effects of butterfly valve positions and core voiding on total recirculation flow, but not the transient flow division among the fuel channels. The total analog simulation utilizes approximately 150 potentiometers, 30 integrators, 50 summers, 12 multipliers, 4 function generators, and 5 relays. The analog circuitry for each of the sections is shown in Sec. 15.

The symbols appearing in the final equations are defined and evaluated in the list at the end of the report. All others are defined in the section in which they appear. In many cases variables are separated into their transient and steady-state parts, denoted by prefix " δ " and subscript "o", respectively. As an example:

$$n = n_o + \delta n$$

2. NEUTRON KINETICS

The transient reactor power is obtained from the net excess reactivity from a set of spatially independent differential equations with time varying coefficients. These equations describe the birth of neutrons a) emitted promptly from fissions, and b) emitted some time after a fission by the decay of fission products. These fission products are divided into six groups according to their decay constants.

Assumptions

1. The neutron population is spatially independent. The axial and radial flux shapes are independent of time and reactor power level.

2. The concentration of fission products with long build-up and decay time constants, such as xenon and samarium, is considered constant.

Derivation

The rate of change of neutron population is given by the equation:

$$\frac{dn}{dt} = \frac{(\delta k_{ex} - 1)\ n}{l^*/\beta} + \sum_{i=1}^{6} \lambda_i\ C_i \qquad (2.1)$$

where δk_{ex} is the excess reactivity in dollars, and the rest of the symbols are defined at the end of the report.

The rate of change of fission product concentration in group "i" is:

$$\frac{dC_i}{dt} = \frac{\beta_i n}{l^*} - \lambda_i\ C_i \qquad (2.2)$$

In Eq. 2.1, δk_{ex} is given by

$$\delta k_{ex} = k_{rods} - k_v - k_d \qquad (2.3)$$

where k_{rods}, k_v, and k_d are reactivity in dollars held in control rods, voids, and fuel temperature, respectively.

Eqs. 2.1 and 2.2 are solved simultaneously on the analog computer using six delayed neutron groups.

3. BOILER FUEL HEAT TRANSFER

The low thermal conductivity of the ceramic boiler fuel pins gives rise to a considerable lag in the transfer of heat to the coolant. The representation of this lag has an appreciable effect on the shape of the system-frequency response

curve, and on several of the safeguards analyses. For these reasons the transient heat transfer is derived in some detail. The assumptions made here are expected to have a minor effect on the accuracy of the heat delivered to the coolant during a transient.

The equation describing the dynamic heat release from a cylindrical, distributed-parameter fuel pin is solved formally using Laplace transforms and Bessel functions. The solution in Laplace form is expanded into an infinite series of partial fractions, each a simple lag. This series is made finite by grouping the shortest lags into one equivalent lag. Three per cent of the power generated is assumed to be carried directly to the coolant by gamma radiation with no lag.

The solutions of these dynamic heat transfer equations are not transformed back into the time domain since the partial-fraction form of the final Eq. 3.13 so readily adapts to analog computer simulation.

Assumptions

1. The UO_2 ceramic is assumed to have cracked and expanded, completely filling the fuel tube with no gap between the UO_2 and the cladding. Accordingly, the thermal conductivity for cracked UO_2, 0.9 Btu/hr-ft-F, is used.

2. The heat capacity of the zirconium cladding is negligible with respect to that of the UO_2.

3. Although the film coefficients in the subcooled and boiling parts of the channel are different, one equivalent value is assumed to exist along the entire length. Because of the presence of subcooled boiling, this assumption is quite good.

4. The thermal conductivity of the cladding and the film coefficient are grouped as one overall heat transfer coefficient, H.

5. Because the radius of the fuel in the upper half of the core is less than the radius in the lower half, a mean square radius is used, weighted by the relative power fractions.

6. The infinite series of terms with time constants less than 0.2 sec are combined into one term with an equivalent time constant. These involve only about 8 per cent of the power generated.

Derivation

The temperature in a power generating medium of thermal conductivity K and diffusivity $\varkappa$ is described by:

$$\nabla^2 \theta + \frac{\dot{Q}_g}{K} = \frac{1}{\varkappa} \frac{d\theta}{dt} \tag{3.1}$$

For a cylinder of radius R with heat transfer coefficient H at its walls, the boundary conditions are:

$$-\frac{d\theta}{dr}\bigg|_R = \frac{H}{K} (\theta - \theta_2) \tag{3.2}$$

and

$$\theta \neq \infty \quad \text{at } r = 0 \tag{3.3}$$

If this problem is solved for the fuel temperature at R, using Laplace transform methods and assuming θ_2 is constant at its saturation value, and the substitutions,

$$\dot{Q}_b(s) = \theta(s,R) \frac{2H}{R} \tag{3.4}$$

$$N \equiv \frac{RH}{K} \tag{3.5}$$

$$T \equiv R^2/\varkappa \tag{3.6}$$

are made, the result is, in Laplace form

$$\dot{Q}_b(s) = \dot{Q}_g(s) \left[\frac{2\, J_1(\sqrt{-Ts})/\sqrt{-Ts}}{J_o(\sqrt{-Ts}) - \frac{\sqrt{-Ts}}{N} J_1(\sqrt{-Ts})} \right] \tag{3.7}$$

where J_1 and J_o are Bessel functions.

Eq. 3.7 may be expanded into a series of partial fractions.

$$\frac{\dot{Q}_b(s)}{\dot{Q}_g(s)} = \sum_{i=1}^{\infty} \frac{F_i}{1+\tau_i s} \tag{3.8}$$

where F_i and τ_i are found from the simultaneous solution of:

$$F_i = \frac{4\, \tau_i/T}{1 + T/\tau_i N^2} \tag{3.9}$$

and

$$N = \sqrt{T/\tau_i} \left[\frac{J_1(\sqrt{T/\tau_i})}{J_o(\sqrt{T/\tau_i})} \right] \tag{3.10}$$

Eq. 3.8 may be made finite by grouping the shorter time constants in one equivalent term:

$$\frac{\dot{Q}_b(s)}{\dot{Q}_g(s)} \simeq \sum_{i=1}^{3} \frac{F_i}{1+\tau_i s} + \frac{1 - \sum_{i=1}^{3} F_i}{1+\bar{\tau}_4 s} \tag{3.11}$$

where

$$\bar{\tau}_4 = \frac{\sum_{i=4}^{\infty} F_i \tau_i/T}{\sum_{i=4}^{\infty} F_i/T} \tag{3.12}$$

Figure 3.1 shows the solution of Eqs. 3.9 and 3.10, and the numerical solution of Eq. 3.12 as functions of N. With the knowledge of N and T, and Figure 3.1, Eq. 3.11 can be evaluated.

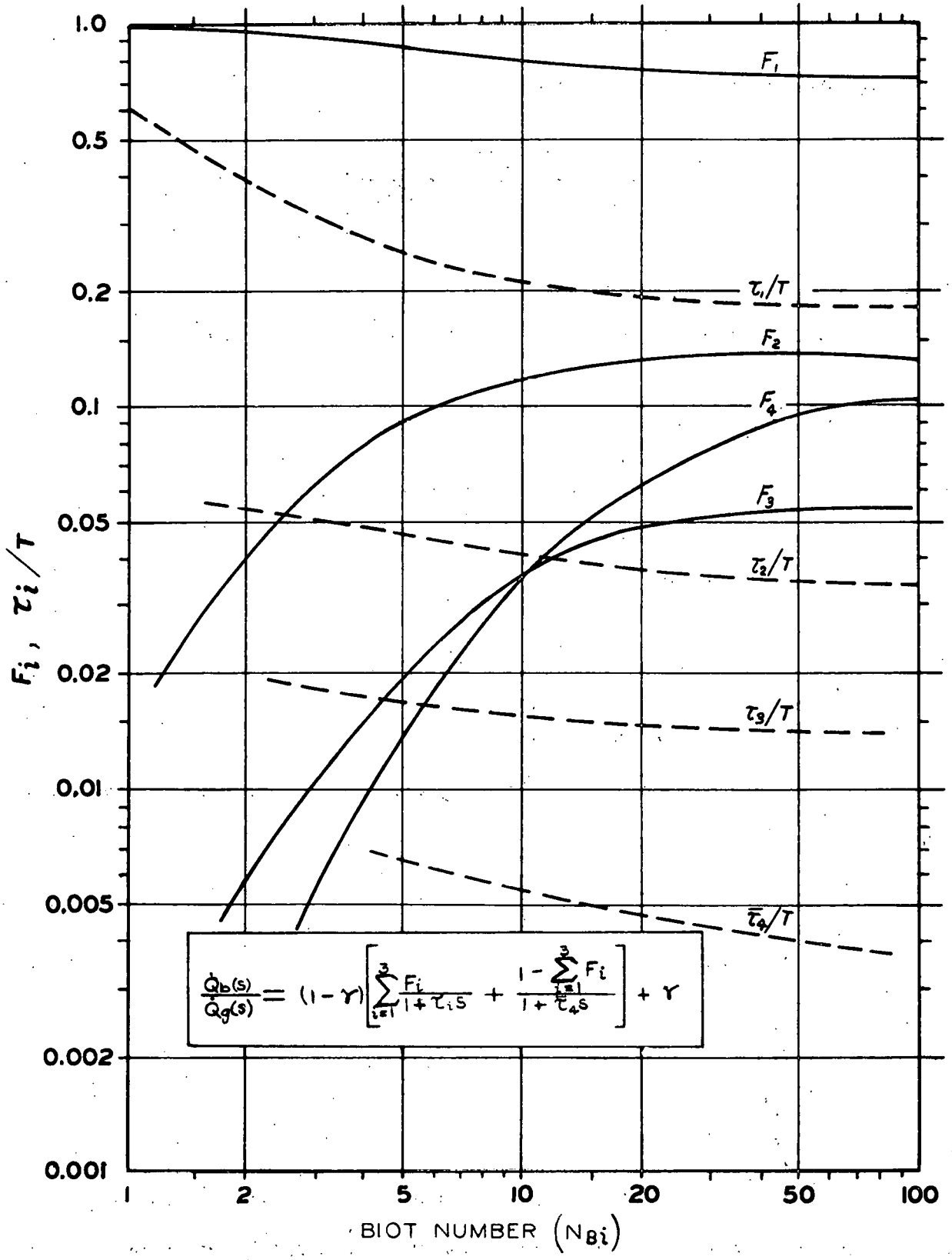

Figure 3.1 Boiler-fuel heat-transfer parameters versus Biot number for cylindrical geometry. (A-C Dwg. 43-024-802)

Since a certain fraction (γ) of the power generated is carried by gammas directly to the coolant, Eq. 3.11 must be corrected:

$$\frac{\dot{Q}_b(s)}{\dot{Q}_g(s)} = (1-\gamma)\left[\sum_{i=1}^{3}\frac{F_i}{1+\tau_i s} + \frac{1-\sum_{i=1}^{3}F_i}{1+\tau_4 s}\right] + \gamma \qquad (3.13)$$

The generated power is directly proportional to the thermal neutron population. Therefore, at all power levels:

$$\frac{\dot{Q}_g(s)}{n(s)} = \frac{\dot{Q}_{go}}{n_o} \qquad (3.14)$$

Eqs. 3.13 and 3.14 are in a form readily adaptable to analog computer simulation, so that they are not inverted from the Laplace domain to the time domain. These two equations are used in the simulation to describe the dynamic heat transfer in the boiler.

Numerical Evaluation

As an example of how the F_i's and τ_i's of Eq. 3.13 are found, the numerical values for these quantities in Pathfinder are calculated. The heat transfer coefficient from the UO_2 to the coolant is:

$$H = \frac{1}{d_c/K_c + 1/h_f} \qquad (3.15)$$

where d_c and K_c are the thickness and thermal conductivity of the cladding. The film coefficient, h_f, is about 6500 Btu/hr-ft^2-F for boiling conditions, and about 3800 Btu/hr-ft^2-F for the subcooled part of the core (assuming some subcooled boiling). Since about 18 per cent of the power is generated in the subcooled part,

$$h_f \simeq 0.82 \times 6500 + 0.18 \times 3800$$

$$= 6000 \text{ Btu/hr-ft}^2\text{-F}$$

Eq. 3.15 is then evaluated

$$H = \frac{1}{.028/(12 \times 7.45) + 1/6000} = 2100 \text{ Btu/hr-ft}^2\text{-F} \qquad (3.16)$$

From the data available on UO_2 thermal conductivity, the estimated value for the cracked, irradiated ceramic is about 0.9 Btu/hr-ft-F.

At the expected full-power operating temperature, the density and specific heat of UO_2 are 636 lbs/ft^3 and 0.073 Btu/lb-F, respectively. Hence,

$$\kappa = \frac{\text{thermal conductivity}}{3600 \times \text{density} \times \text{specific heat}} = \frac{0.9}{3600 \times 636 \times .073}$$

$$= 5.4 \times 10^{-6} \text{ ft}^2/\text{sec} \qquad (3.17)$$

The fuel pellet radii are different in the upper and lower halves of the core. The equivalent radius is:

$$R = \sqrt{\frac{\%\dot{Q}_b}{100} \text{ lower} \times R^2 \text{ lower} + \frac{\%\dot{Q}_b}{100} \text{ upper} \times R^2 \text{ upper}}$$

$$= \sqrt{0.4\ (.013)^2 + 0.6\ (.0146)^2} = 0.0140 \text{ ft.} \qquad (3.18)$$

From Eqs. 3.16, 3.17, and 3.18, N and T are:

$$N = \frac{RH}{K} = \frac{0.014 \times 2100}{0.9} = 32.8$$

$$T = \frac{R^2}{\kappa} = \frac{(0.014)^2}{5.4 \times 10^{-6}} = 36.3 \text{ sec.}$$

Using these values with Figure 3.1, F_i, τ_i, and $\bar{\tau}_4$ in Eq. 13.13 are evaluated. The boiler heat transfer relation for Pathfinder becomes:

$$\frac{\dot{Q}_b(s)}{\dot{Q}_g(s)} = \frac{0.71}{1 + 6.8s} + \frac{0.13}{1 + 1.27s} + \frac{0.05}{1 + 0.51s} + \frac{0.08}{1 + 0.16s} + .03 \qquad (3.19)$$

4. REACTIVITY CHANGE DUE TO THE DOPPLER EFFECT

An increase in fuel temperature causes a broadening of the resonance peaks in the U^{238} cross section spectrum, resulting in more neutron captures during the slowing down process. This reactivity change, called the Doppler effect, can be directly associated with average fuel temperature, and considered quite independent of moderator conditions.

Assumptions

1. Boiling conditions always prevail, and the average fuel temperature never goes below 489 F

2. The boiler-fuel thermal properties are constant between 489 F and 1200 F.

3. The Doppler reactivity is linear with average fuel temperature between 489 F and 1200 F. (See Figure 4.1)

Derivation

The rise of the average boiler fuel temperature from the channel saturation value (489 F) is:

$$\Delta T_{avg} = \frac{1}{C} \int_o^t (\dot{Q}_g - \dot{Q}_b)\, dt \qquad (4.1)$$

where C is the total fuel heat capacity, and $\dot{Q}_g$ is the boiler power generated in the fuel, and $\dot{Q}_b$ is the boiler power transferred to the coolant.

If k_d is defined as the change in reactivity due to Doppler effect as the average fuel temperature rises above 489 F, assumption 3 permits:

$$\frac{\partial k_d}{\partial T_{avg}} = \text{constant} \qquad (4.2)$$

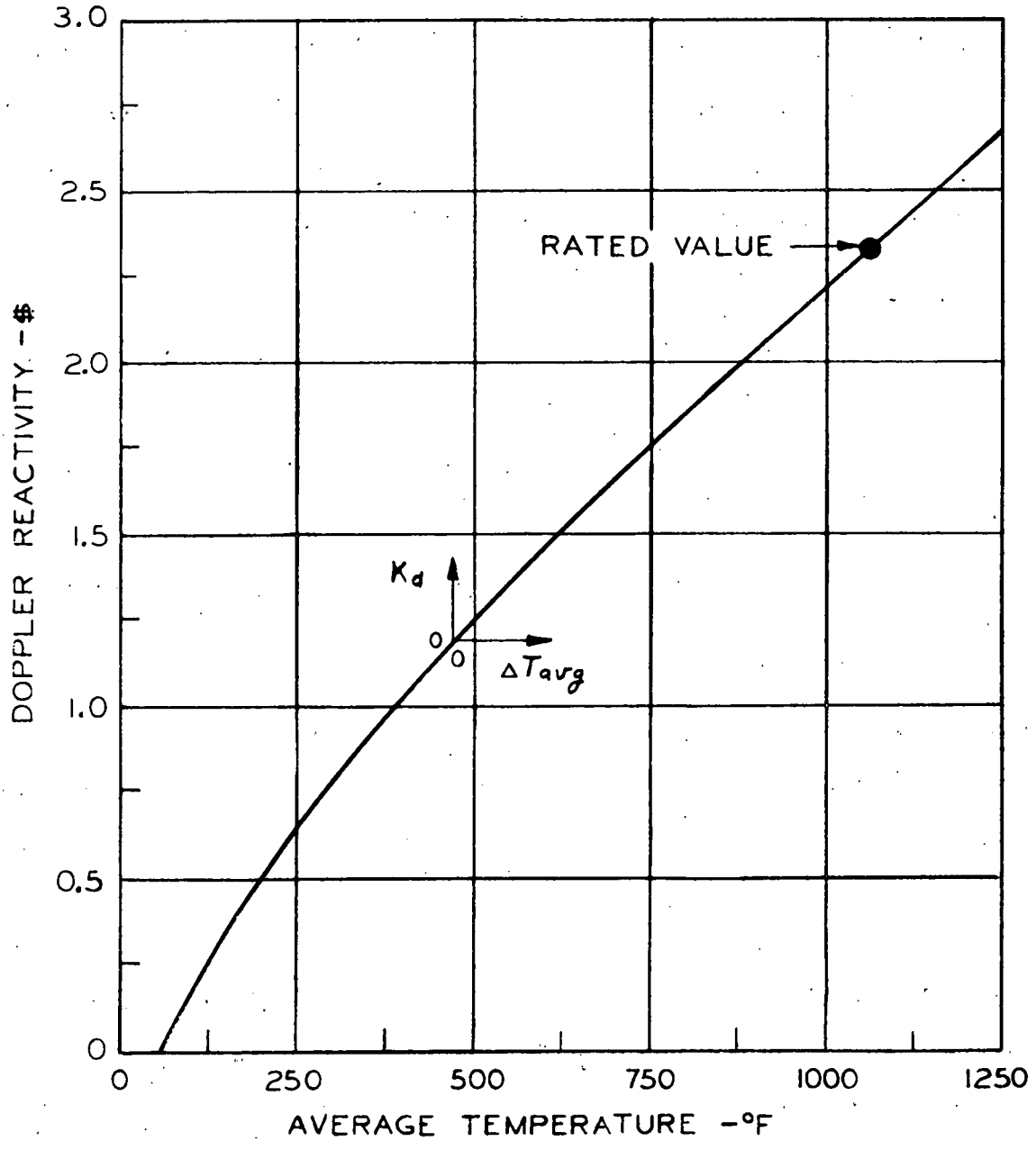

Figure 4.1 Doppler reactivity versus average boiler fuel temperature. (A-C Dwg. 43-024-786)

From Eqs. 4.1 and 4.2

$$k_d = \left[\frac{\partial k_d}{\partial T_{avg}}\right] \frac{1}{C} \int_o^t (\dot{Q}_g - \dot{Q}_b)\, dt \qquad (4.3)$$

5. ENERGY AND VOLUME MASS BALANCE OF SATURATED PART OF PRIMARY SYSTEM

The rate of change of reactor pressure results from an unbalance of the mass and energy entering and leaving the primary system. In calculating the energy balance, it is important to differentiate between the saturated and subcooled water in the system. For simplicity, the vessel and recirculation loops are treated in two parts: (A) a control volume including the saturated steam and water in the vessel, and (B) a control volume including the subcooled primary water between the feedwater ring and the active core inlet. The first will be taken here, the second in Sec. 6.

Assumptions

1. The control volume, or volume of saturated water and steam remains constant.

2. During both pressure rises and drops, all the saturated water and steam remain saturated, and enthalpy and specific volume follow the saturation line.

Derivation

a) Mass balances

Referring to Figure 5.1, the rate of change of mass of saturated water is

$$\dot{M}_f = W_v - W_d - W_{fg} \qquad (5.1)$$

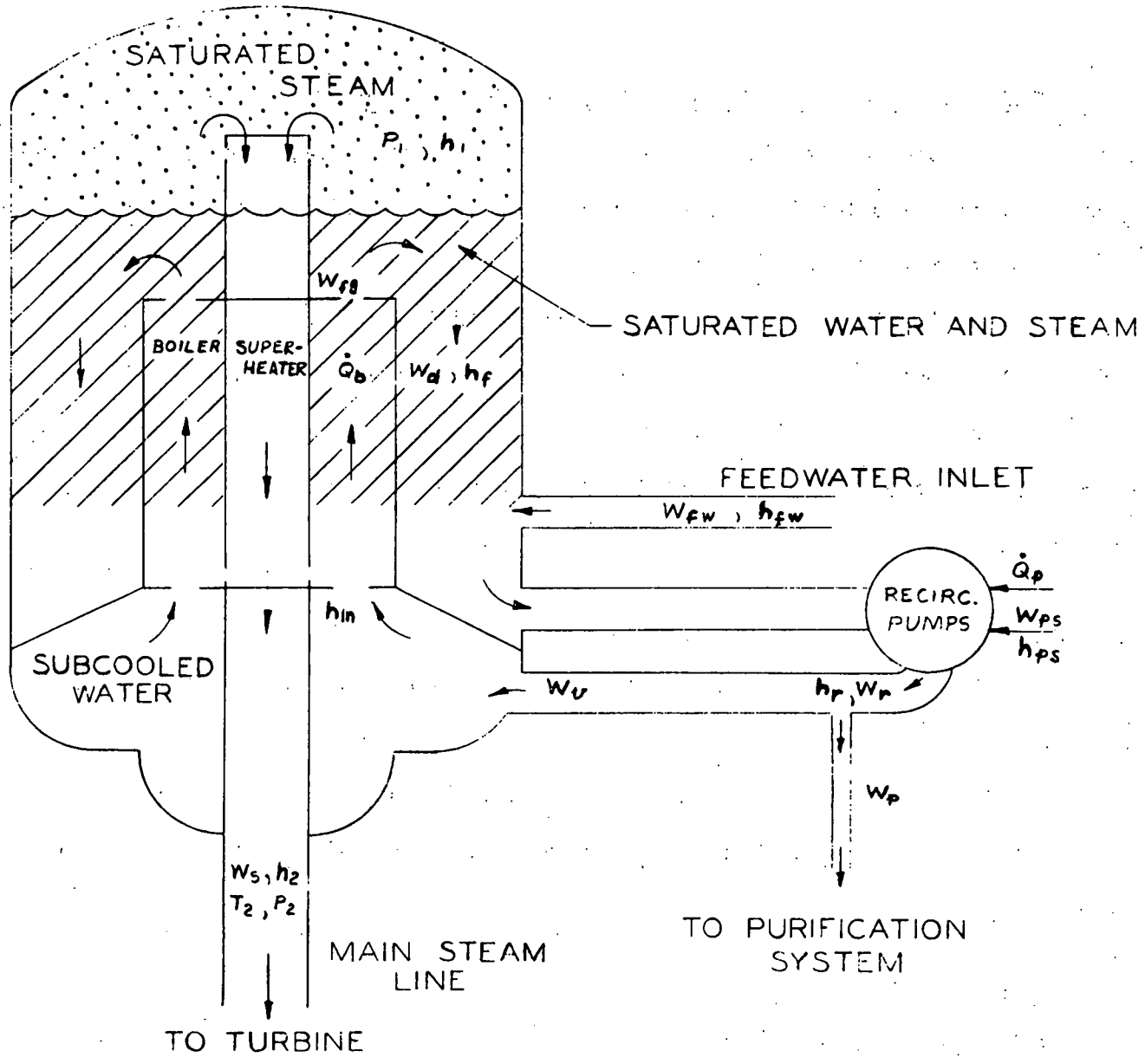

Figure 5.1 Thermal schematic of primary system. (A-C Dwg. 43-024-710)

and of saturated steam:

$$\dot{M}_g = W_{fg} - W_s \tag{5.2}$$

b) Volume Balance

The volume of saturated water and steam is:

$$V_{sat} = M_f v_f + M_g v_g \tag{5.3}$$

where v_f and v_g are specific volumes of the saturated water and steam, respectively.

From assumption 1:

$$\dot{V}_{sat} = M_f \dot{v}_f + M_g \dot{v}_g + v_f \dot{M}_f + v_g \dot{M}_g = 0 \tag{5.4}$$

c) Energy Balance

$$\dot{Q}_b + \dot{Q}_m + h_{in} W_v - h_g W_s - h_f W_d = \frac{d}{dt}(u_f M_f + u_g M_g)$$

$$= M_f \dot{h}_f + M_g \dot{h}_g + h_f \dot{M}_f + h_g \dot{M}_g - \frac{V_{sat}\,\dot{P}_l}{J} \tag{5.5}$$

where $\dot{Q}_b$ is power transferred to boiler coolant,

$\dot{Q}_m$ is power transferred out of active boiler core,

v_f, v_g, h_f, h_g are the internal energy and enthalpy of the saturated water and steam, respectively.

J is an energy conversion factor.

Combining Eqs. 5.1, 5.2, 5.4, and 5.5 to eliminate $\dot{M}_f$, $\dot{M}_g$, and W_{fg}, and making the substitutions, $\Delta h = h_f - h_{in}$ and $W_v - W_d = W_{fw} + W_{ps} - W_p$, (See Figure 5.1) then,

$$\frac{dP_l}{dt} = \frac{\dot{Q}_b + \dot{Q}_m - W_v \Delta h - \left(1 + \frac{v_f}{v_{fg}}\right) h_{fg} W_s + \frac{h_{fg} v_f}{v_{fg}} (W_{fw} + W_{ps} - W_p)}{M_f \left(\frac{\partial h_f}{\partial P} - \frac{h_{fg}}{v_{fg}} \frac{\partial v_f}{\partial P}\right) + M_g \left(\frac{\partial h_g}{\partial P} - \frac{h_{fg}}{v_{fg}} \frac{\partial v_g}{\partial P}\right) - \frac{V_{sat}}{J}} \tag{5.6}$$

Numerical Evaluation

Due to uncertainties in evaluating the saturated portion of fluid in the steam separator region, maximum and minimum values of the denominator of Eq. 5.6 (defined as "D") are calculated. Using the minimum saturated water mass of 32,400 lbs and total saturated volume of 1424 ft^3:

$$D_{min}=32,400\ (0.205-\frac{728}{0.732}\times 3.75\times10^{-6})+\ 1025(\frac{728}{0.732}\times 1.25\times 10^{-3}-0.017)-\frac{1424}{5.4}$$

$$= 749!\ \text{Btu/psi} \qquad (5.7)$$

Using the maximum saturated water mass of 47,500 lbs and total saturated volume of 1729 ft^3:

$$D_{max} = 10,485\ \text{Btu/psi} \qquad (5.8)$$

The best estimate is considered to be 34,200 lbs and 1460 ft^3, which gives a "D" of:

$$D_i = 8000\ \text{Btu/psi} \qquad (5.9)$$

6. ENERGY AND MASS BALANCES OF SUBCOOLED PART OF PRIMARY SYSTEM

The temperature and flow rate of the water entering the bottom of the boiler core has an appreciable effect on the core dynamics. The water temperature just below the feedwater ring immediately reflects any changes in vessel pressure, flow rates, or temperatures. However, a transport time must be allowed for this water to flow through the recirculation system before the temperature change is felt at the core inlet. In this section, dynamic core inlet subcooling is obtained as a function of the system flow rates, reactor pressure, and feedwater temperature.

Assumptions

1. Volume of subcooled water is constant.
2. Subcooled water is incompressible.
3. Purification out-flow, pump-seal in-flow, and pump energy given to fluid are constant and occur at feedwater ring rather than at their actual locations.
4. Changes in local pressure are equal to changes in reactor dome pressure.
5. Recirculation transit time is constant during a process.

Derivation

a) Energy and mass balances at feedwater ring

The flow continuity equation at the point of the feedwater ring is:

(see assumption 3 and Figure 5.1)

$$W_v = W_d + W_{ps} + W_{fw} - W_p \tag{6.1}$$

The energy rate balance is:

$$h_r W_v = h_f W_d + h_{ps} W_{ps} + h_{fw} W_{fw} - h_r W_p + \dot{Q}_p \tag{6.2}$$

where $\dot{Q}_p$ is the energy rate given to the water by the pump.

Combining Eqs. 6.1 and 6.2:

$$h_r = h_f - \frac{W_{fw}(h_f - h_{fw}) + W_{ps}(h_f - h_{ps}) - \dot{Q}_p}{W_v + W_p} \tag{6.3}$$

b) Energy balance of subcooled control volume:

During transients, the internal energy of the subcooled control volume, (i.e., the volume of water between the feedwater ring and the core inlet, including the recirculation lines and lower vessel plenum) is not the same throughout. Therefore, this volume is broken up along the flow path into an infinite number of sections of infinitesimal length, each of which has a volume, ΔV. An energy balance for one of these sections is, using assumptions 2, 3, and 4:

$$W_v (h_{i-1} - h_i) = \dot{U} = \rho \Delta V \dot{h}_i - \frac{\Delta V}{J} \dot{P}_i \tag{6.4}$$

where h_i and h_{i-1} are the enthalpies at the outlet and inlet of the i^{th} section;

$\dot{U}$ is the rate of change of internal energy in the section;

ρ is the density of the water and

J is an energy conversion factor.

Eq. 6.4 is written for each section, and this infinite set of equations is solved for the enthalpy at the outlet of the last section. The outlet enthalpy of the last section (which is also the core inlet enthalpy, h_{in}) can then be written as a function of the enthalpy of the first section, h_r, and reactor pressure, P_l:

$$h_{in}(t) = h_r(t - T_r) + \frac{P_l(t)}{\rho J} - \frac{P_l}{\rho J}(t-T_r) \qquad (6.5)$$

where T_r, the transport time through the entire subcooled control volume is considered a constant according to assumption 5.

Finally the subcooling at the core inlet is,

$$\Delta hW_v = (W_r - W_p)(h_f - h_{in}) \qquad (6.6)$$

where h_{in} is obtained from Eqs. 6.3 and 6.6, and

Δh is defined as $h_f - h_{in}$.

In the derivation of Eq. 6.5 a flat velocity profile was assumed for the fluid in the volume between the feedwater ring and the core inlet. Actually, some undetermined amount of mixing will occur just below the feedwater ring and in the recirculation piping, so that a parabolic velocity profile will probably exist. Cold feedwater would actually be seen at the core inlet gradually, rather than suddenly as the equation states. Thus, the pure delay indicated by the $(t-T_r)$ function should be a smoother function. As explained in Sec. 15, the actual simulation of this delay phenomenon is smoother than that indicated by Eq. 6.5.

To increase the accuracy of the analog simulation, the variables and equations are broken up into a steady-state and a variable component, e.g., $P_l = P_{l_o} + \delta P_l$:

Keeping only the transient part of Eq. 6.3 and rearranging:

$$W_{ro}\delta h_r = (W_{ro}-W_{fwo}-W_{pso})\ \delta h_f + (h_{fo}-h_{ro})\ \delta W_r + (\delta W_r-\delta W_{fw})\ \delta h_f - (h_{fo}-h_{fwo})\ \delta W_{fw} + \delta W_{fw}\delta h_{fw} + W_{fwo}\delta h_{fw} - \delta W_r\delta h_r \quad (6.7)$$

The transient part of Eq. 6.5 is:

$$W_{ro}\delta h_{in}(t) = W_{ro}\delta h_r(t-T_r) - \frac{W_{ro}}{\rho J}\delta P_l(t-T_r) + \frac{W_{ro}}{\rho J}\delta P_l(t) \quad (6.8)$$

where Δh_o is evaluated from the steady-state solutions of 6.3 and 6.5 as

$$\Delta h_o = h_{fo} - h_{ino} = h_{fo} - h_{ro} = \frac{W_{fwo}}{W_{ro}}(h_{fo} - h_{fw}) + \frac{W_{pso}}{W_{ro}}(h_{fo} - h_{pso}) - \dot{Q}_p \quad (6.9)$$

Thus, $W_v\Delta h$ is generated in the simulator from Eqs. 6.6, 6.7, 6.8, and 6.9.

7. REACTIVITY IN VOIDS

Voids in the boiler-core moderator increase the fuel-to-moderator ratio and decrease the core reactivity. The reactivity decrease due to boiler voids can be expressed as a function of inlet flow, subcooling, and boiler power. The voids in the superheater moderator have been found to have a negligible effect on reactivity, so they are neglected here.

Assumptions

1. Axial power shape is the same regardless of subcooling or power level, as long as no more than 40 per cent of the power is used to saturate the coolant.

2. In calculating the effective void fraction, the local coefficient,

$\partial k_{eff}/\partial x$, is constant in the lower core half, and constant at 68 per cent of this value in the upper core half.

3. The axial fast flux is the proper void weighting function.

Although under some conditions the validity of these assumptions may be questioned, the net effect on the results of this section is minor.

Derivation

a) Mean Effective Steam Fraction by Weight

The effective steam fraction is the actual steam fraction multiplied by the local void-reactivity importance function shown in Figure 7.3. Thus, the mean effective steam weight-fraction is:

$$\bar{x} = \int_{z_o}^{1} \varphi_1'(z)\, x(z)\, dz \qquad (7.1)$$

and,

$$x(z) = x_e \frac{[\dot{Q}(z) - \dot{Q}(z_o)]}{1 - \dot{Q}(z_o)} \qquad (7.2)$$

where, z is fraction of core height measured from the bottom,

z_o is position of boiling incidence,

$x(z)$ is the steam fraction by weight at position z,

x_e is steam fraction at core exit,

$\dot{Q}(z)$ is fraction of core power generated below z, and is assumed to be a function of z only (assumption 1). See Figure 7.4.

$\varphi_1'(z)$ is the local void-reactivity importance function, and according to assumptions 2 and 3, is the fast neutron flux for $z < 0.5$, and 0.68 times the fast flux for $z > 0.5$, normalized such that $\int_0^1 \varphi_1'(z)dz = 1.0$.

Eqs. 7.1 and 7.2 were combined and numerically integrated (using Figures 7.3 and 7.4). A change of variable

$$\frac{\dot{Q}(z_o)}{1-\dot{Q}(z_o)} = \frac{\Delta h}{x_e h_{fg}} \tag{7.3}$$

is made; where, Δh is the enthalpy of subcooling, and h_{fg} is the heat of vaporization. The resultant function is approximated by

$$\bar{x} = I\, x_e - E\, \frac{\Delta h}{h_{fg}} \tag{7.4}$$

where, $I = \int_o^l \varphi_l'(z)\, \dot{Q}(z)\, dz = 0.537$, and

E, graphically evaluated, is 0.375.

Eq. 7.4 does not consider the dynamics of void formation. Hence,

$$\bar{x}(s) = \bar{x}\, g(s) \tag{7.5}$$

where, g(s) is derived in the next section.

The exit void weight-fraction, x_e, is generated from the equations:

$$x_e = W_{fg}/W_w \tag{7.6}$$

and

$$W_{fg} = \frac{\dot{Q}_b - \Delta h W_w}{h_{fg}} - \frac{\partial W_{fg}}{\partial \dot{P}_l}\, \dot{P}_l \tag{7.7}$$

where, $\partial W_{fg}/\partial \dot{P}_l$ is derived in Sec. 9.

b) Mean Effective Steam Fraction by Volume

The relationship between steam fraction by weight and volume depends on the pressure, the channel geometry, and coolant velocity. Experimental data for conditions similar to Pathfinder indicate that the Modified Martinelli relationship (Figure 7.1) would probably be the best estimate for the steam volume-fraction-to-weight-fraction relation.

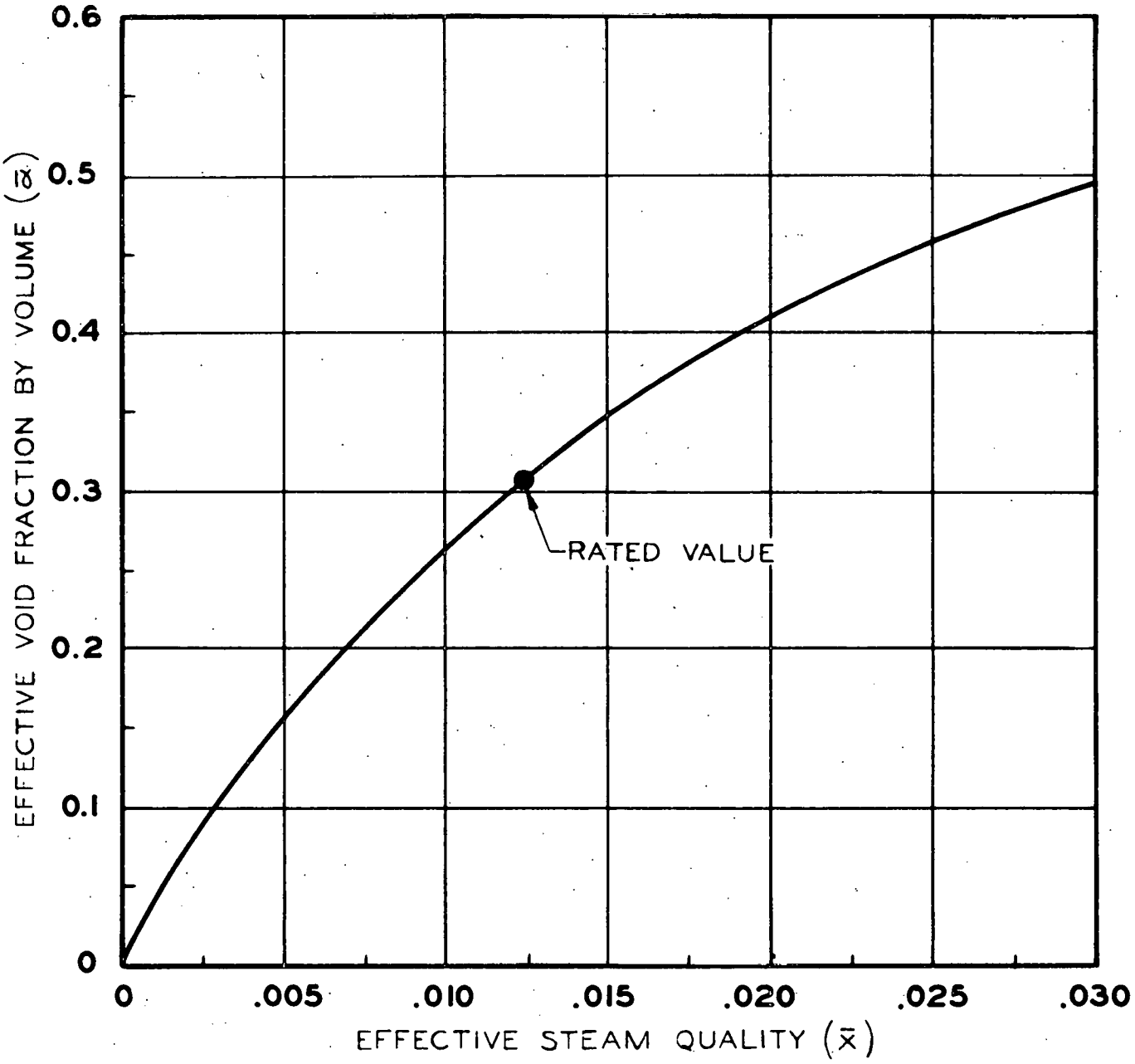

Figure 7.1 Modified Martinelli void-quality relation. (A-C Dwg. 43-024-753)

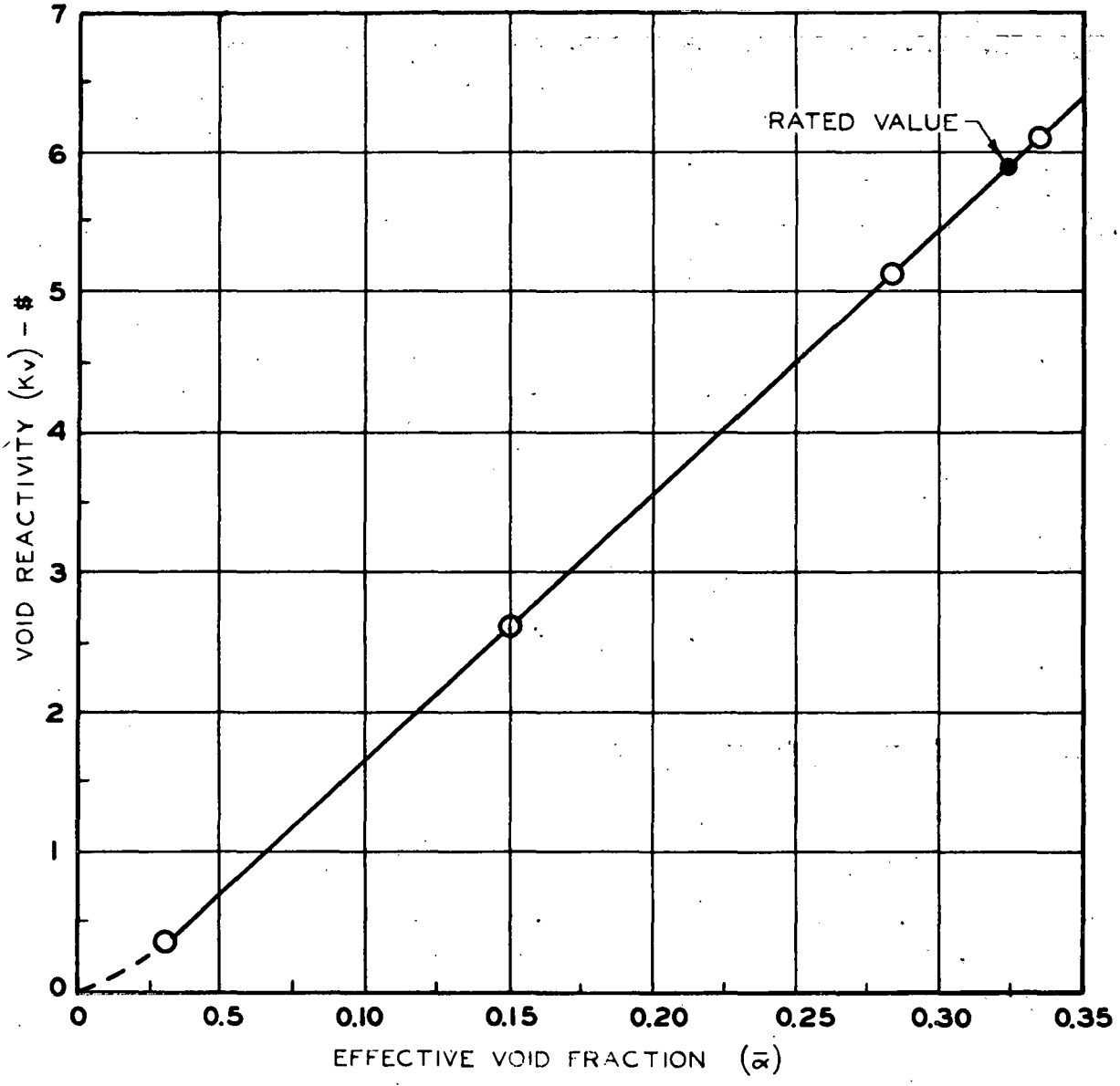

Figure 7.2 Reactivity in voids versus effective void fraction. Plotted points were obtained from PDQ code. (A-C Dwg. 43-024-754)

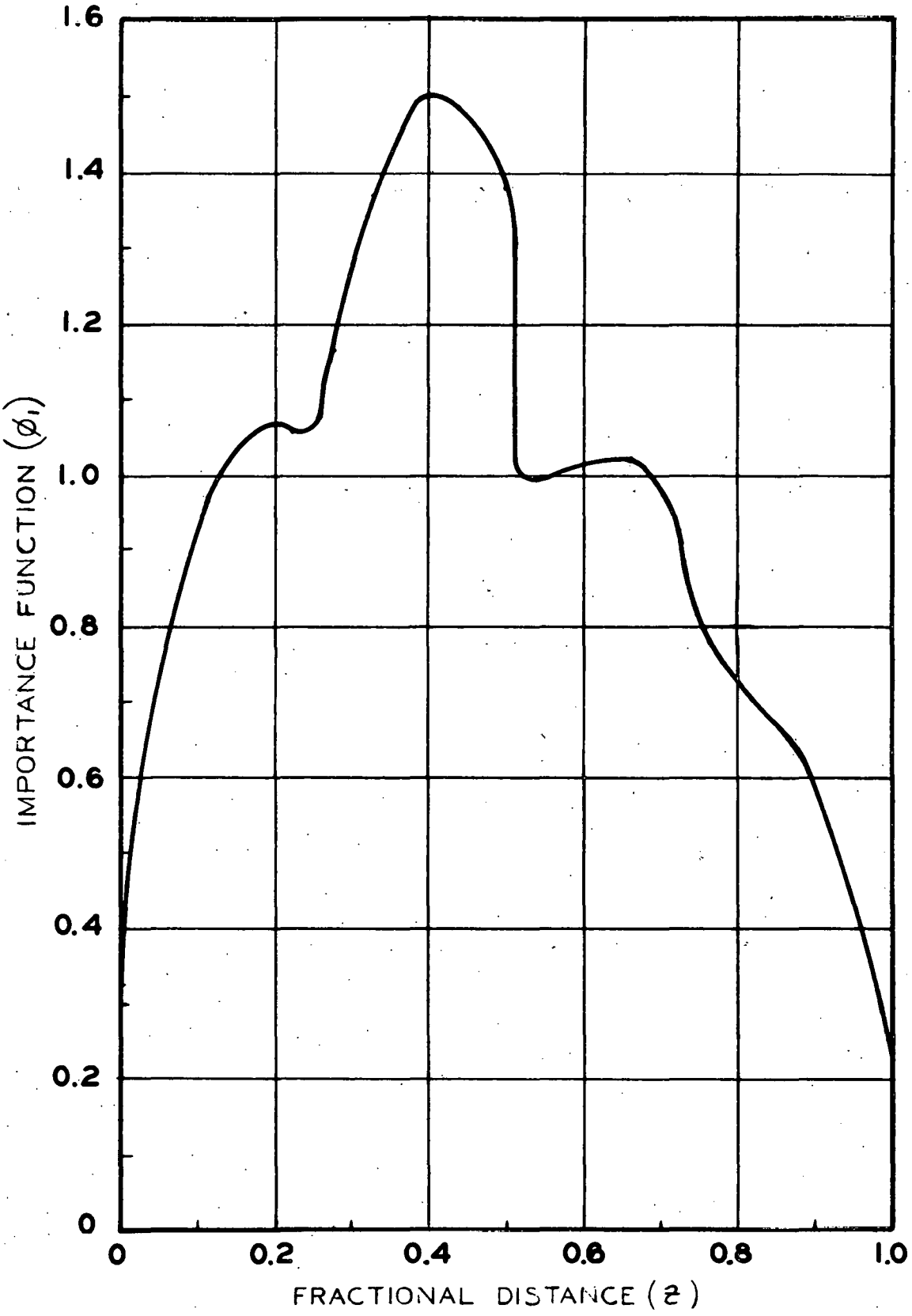

Figure 7.3 Local void-reactivity importance versus distance from bottom of core. (A-C Dwg. 43-024-758)

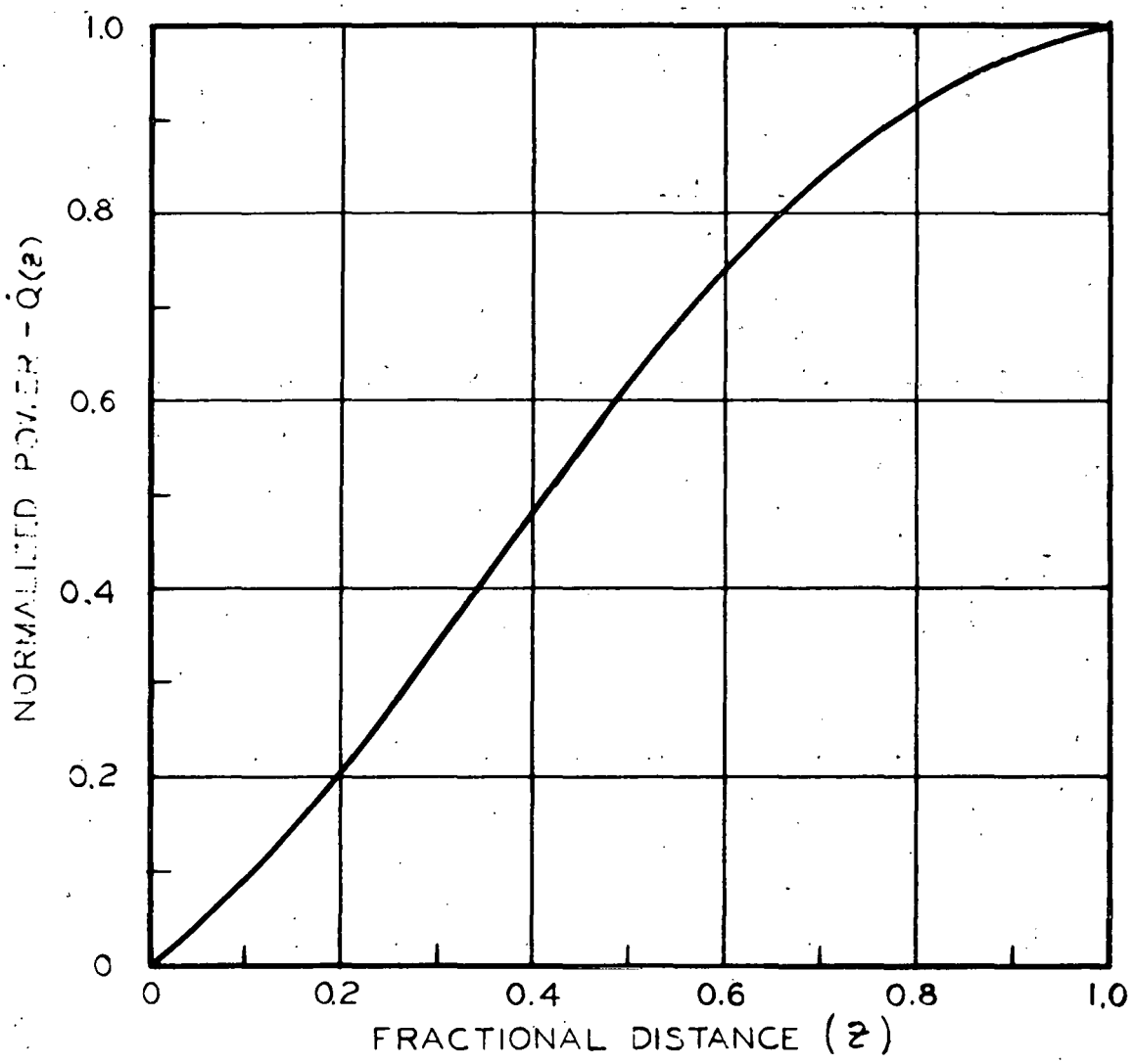

Figure 7.4 Fraction of total boiler power versus distance from bottom of core. (A-C Dwg: 43-024-755)

c) Reactivity In Voids

Various core conditions with widely different values of inlet subcooling and power level were used as inputs to the PDQ code on the IBM 704 Computer from which the values of reactivity in voids were obtained. For each of these core conditions, the mean effective void volume-fraction was calculated as in "a" and "b" above. Figure 7.2 shows these void volume-fractions plotted against the reactivity obtained from the PDQ problems. The reactivity coefficient is quite constant at 19.1 $/α.

The relations simulated are Eqs. 7.4, 7.5, 7.6 and 7.7; Figures 7.1 and 7.2.

8. VOID REDISTRIBUTION DYNAMICS

If boiler core power or subcooling change suddenly, the axial void distribution will change according to the equations in Sec. 7, changing the core reactivity. However, the total reactivity held in voids does not change suddenly to a new value after the disturbance, because the newly formed voids must be washed up the core before a new steady-state distribution can exist. Thus, a certain time lag, associated with the core void-transport time, must be accounted for in calculating the void changes in the core.

Assumptions

1. All assumptions of Sec. 7 apply.

2. The function g(s) is derived for void disturbances resulting from power changes only, but the result is also applied to disturbances resulting from subcooling changes.

3. The axial core boiling length was taken as eight sections, with conditions assumed uniform throughout a section.

Derivation

Consider an impulse in boiler core power variation. The void distribution will not return to its original condition until the new voids formed at each axial core position have been washed out of the core. The new voids formed at core position z (fraction of core height above bottom) will have been washed out after a time $\tau(z)$, where,

$$\tau(z) = \int_z^1 \frac{dz}{v(z)} \tag{8.1}$$

and v(z) is steam velocity in core-height-per-second. This is considered a transport lag. The Laplace transform is used to include this dynamic effect in Eq. 7.1:

$$\bar{x}(s) = \int_{z_o}^1 \varphi_1'(z)\, x(z) e^{-\tau(z)s}\, dz \tag{8.2}$$

where, the symbols other than $\tau(z)$ are defined in Sec. 7, and $\dot{Q}(z_o)$ is considered constant for the purposes of this transient effect (assumption 2).

From Eq. 7.5 and 8.2 the transfer function g(s) is:

$$g(s) = \int_{z_o}^1 \Psi(z) e^{-\tau(z)s} dz \tag{8.3}$$

where, from the relations derived in Sec. 7:

$$\Psi(z) = \frac{\varphi_1'(z)\,[\dot{Q}(z) - \dot{Q}(z_o)]}{\int_{z_o}^1 \varphi_1'(z)\,[\dot{Q}(z) - \dot{Q}(z_o)]dz} \tag{8.4}$$

To facilitate the solution of Eq. 8.3, the core is broken down into eight axial sections, Eq. 8.3 being expressed as a summation instead of an integral, and the perfect lag is approximated such that Eq. 8.3 can be written as:

$$g(s) \simeq \sum_{i=1}^{8} \Psi_i \frac{(1 - \tau_i s)}{(1 + \tau_i s)} \tag{8.5}$$

where,

$$\Psi_i = \int_{z_o + (i-1)\frac{(1 - z_o)}{8}}^{z_o + \frac{i(1 - z_o)}{8}} \Psi(z)\, dz \tag{8.6}$$

and

$$\tau_i = \int_{z_o + (i-1)\frac{(1 - z_o)}{8}}^{z_o + \frac{i(1 - z_o)}{8}} \frac{dz}{v(z)} \tag{8.7}$$

Numerical Evaluation

The values of τ_i and Ψ_i were calculated from Eqs. 8.4, 8.6, 8.7 using Figures 7.3 and 7.4 and a steam velocity $v(z)$ given by Eq. 8.8.

$$v(z) = 4.33\ z\ \text{sec}^{-1} \tag{8.8}$$

Examination of Figure 8.1 shows that one single lag with a break frequency of 20 radians/second is a good approximation to the more exact Eq. 8.5 in the frequency range of interest. Thus, Eq. 8.9 is the relation simulated that

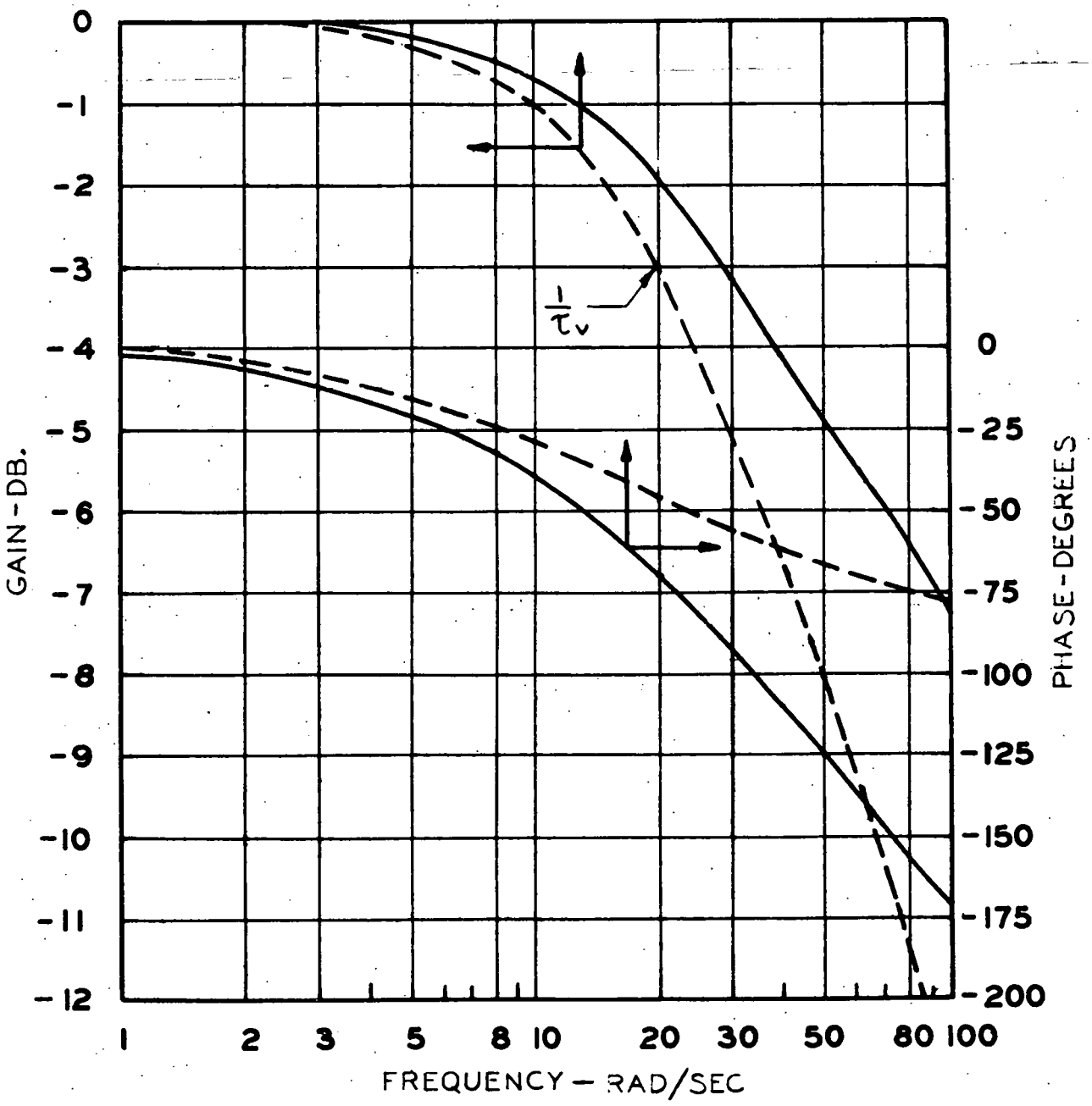

Figure 8.1 Bode plot of void redistribution transfer function. Solid curve is exact according to Eq. 8.3. Dashed curve is from simulation of Eq. 8.9. (A-C Dwg. 43-024-805)

accounts for the dynamics of void redistribution.

$$g(s) \simeq \frac{1}{1 + \tau_V s} \tag{8.9}$$

9. PRESSURE EFFECTS ON REACTIVITY

The boiler-core pressure can affect the moderator density, and, thus, the core reactivity, in three ways:

1) The static reactivity coefficient due to changes in steam bubble size and water temperature and density, which depends upon the magnitude of the pressure.

2) The transient coefficient, which includes the changes in amount of steam voids because of flashing or condensation resulting from a rate of pressure change.

3) Changes in core inlet subcooling, or core non-boiling length. This effect was treated in Sec. 6.

Assumptions

1. The mean void fraction by volume is equal to the mean effective void fraction by volume (See Sec. 7).

2. Changes in the steam dome pressure are the same as those in the boiler core pressure.

3. The normally saturated core water and steam always follow the saturation lines.

4. The results are linearized about 615 psia.

Derivation

a) Static Effect

The reactivity coefficient due to pressure effects on channel density is:

$$\frac{\partial k_v}{\partial P_1} = \frac{\partial k_v}{\partial \bar{\alpha}} \frac{\partial \bar{\alpha}}{\partial \rho_c} \frac{\partial \rho_c}{\partial P_1} \tag{9.1}$$

where, the channel density, ρ_c, is

$$\rho_c = \frac{(1 - \bar{\alpha})}{v_f} + \frac{\bar{\alpha}}{v_g} \simeq \frac{(1 - \bar{\alpha})}{v_f} \tag{9.2}$$

the void fraction by volume, $\bar{\alpha}$, is

$$\bar{\alpha} = \frac{1}{1 + \frac{v_f}{v_g} S \left(\frac{1}{\bar{x}} - 1\right)} \simeq \frac{1}{1 + \frac{v_f \, S h_{fg}}{v_g \, \bar{x} h_{fg}}} \tag{9.3}$$

where:

v_f and v_g are the specific volumes of saturated water and steam,

h_{fg} is the heat of vaporization per pound,

S is the channel slip ratio,

$\bar{x}$ is the total steam fraction by weight, and

P_1 is the core pressure (see assumption 2).

From Eq. (9.2):

$$\frac{\partial \bar{\alpha}}{\partial \rho_c} = -v_f \tag{9.4}$$

Remembering that the product $h_{fg}\bar{x}$ is independent of pressure, from Eqs. 9.2 and 9.3 it can be shown that

$$\frac{\partial \rho_c}{\partial P_1} = - \frac{(1 - \bar{\alpha})}{v_f} \left[\bar{\alpha} \left(\frac{1}{v_f} \frac{\partial v_g}{\partial P_1} - \frac{1}{h_{fg}} \frac{\partial h_{fg}}{\partial P_1} \right) + \frac{(1 - \bar{\alpha})}{v_f} \frac{\partial v_f}{\partial P_1} \right] \tag{9.5}$$

Substituting Eqs. 9.4 and 9.5 into Eq. 9.1:

$$\frac{\partial k_v}{\partial P_l} = -\frac{\partial k_v}{\partial \bar{\alpha}}(1-\bar{\alpha})\left[\bar{\alpha}\left(\frac{1}{v_g}\frac{\partial v_g}{\partial P_l} - \frac{1}{h_{fg}}\frac{\partial h_{fg}}{\partial P_l}\right) + \frac{(1-\bar{\alpha})}{v_f}\frac{\partial v_f}{\partial P_l}\right] \qquad (9.6)$$

To simplify the analog circuitry, the $(1-\bar{\alpha})$ factor in front of the bracket is considered constant, so that $\partial k_v/\partial P_l$ becomes a linear function of $\bar{\alpha}$.

b) Transient Effect

Taking the control volume as the saturated water and steam in the core, and assuming core power and subcooling constant, Eq. 5.6 can be applied to the core, giving

$$\frac{\partial W_{fg}}{\partial P_l} = -\frac{D'}{h_{fg}\left(1+\frac{v_f}{v_{fg}}\right)} \qquad (9.7)$$

where, D' is evaluated just as D was in Sec. 5, except that the masses and volume apply to the core only. W_{fg} is the core exit steam flow.

Eq. 9.7 is used to evaluate Eq. 7.7.

Using the values for the boiler core, D' is calculated:

$$D' = 2100\left(0.2 - 3.5\times10^{-6}\times\frac{728}{0.73}\right)$$

$$+ 11.7\left(-0.018 + 1.2\times10^{-3}\times\frac{728}{0.73}\right) - \frac{53}{5.4} = 416 \text{ Btu/psi}$$

and Eq. 9.7 becomes

$$\frac{\partial W_{fg}}{\partial P_l} = \frac{-416}{728\left(1+\frac{.0202}{.73}\right)} = -0.57 \qquad (9.8)$$

10. SUPERHEATER TEMPERATURES

The superheater fuel elements contain their fuel as a UO_2-stainless steel cermet in two concentric annuli with stainless steel cladding. Steam flows on either side of each annulus in three annular steam spaces. (See figure 10.1) Although temperatures at various points of the superheater are widely different, the only two positions of interest in dynamics studies are the hot spot and the superheater exit. Hot spot data (including wire spacer effects) were obtained from heat transfer studies on the digital computer for the reference design of 750 F maximum exit steam temperature. The equations derived here use these data to give the transient temperatures at the hot spot and superheater exit as functions of neutron flux and steam flow. This simulation is greatly simplified by the fact that the superheater-temperature reactivity coefficients are negligible.

Assumptions

1. The neutron flux level throughout the superheater varies uniformly with the total reactor flux level.

2. Reactivity coefficients in the superheater are negligible as compared with those in the boiler.

3. Fluctuations in the amount of heat transferred by radiation are negligible.

4. The thin fuel tubes can be described with lumped parameter, flat plate geometry.

5. The heat transfer coefficients are functions of steam flow only.

6. The steam heat capacity is negligible as compared to that of the fuel.

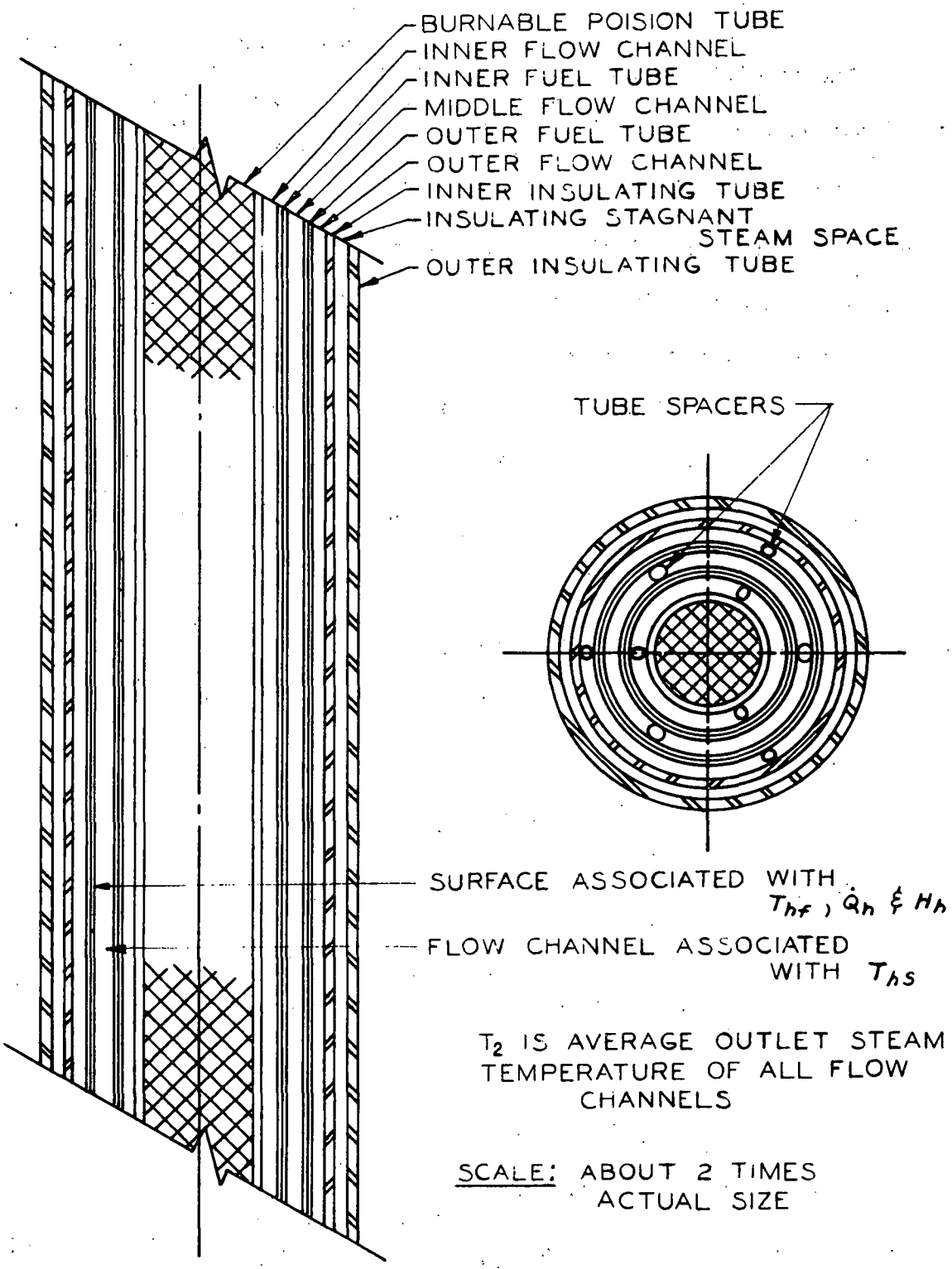

Figure 10.1 High-enrichment superheater fuel element.
(A-C Dwg. 43-024-803)

7. The specific heat of the steam at the hot spot and at the exit are constant during the expected temperature and pressure variations.

8. The steam enthalpy at the inlet is constant.

Physics calculations indicate that assumptions 1 and 2 are within the accuracy of the overall simulation for reasonable power fluctuations. Assumption 3 is valid except at very low power levels (< 1 per cent of full power). With regard to assumption 5, the uncertainties in the absolute value of the heat transfer coefficients make a temperature correction illogical. The remaining assumptions do not appreciably affect the accuracy of the results.

Derivations

Considering a lumped-parameter fuel tube, the energy balance across the fuel surface at some axial point (taken here as the hot spot) is:

$$\dot{Q}_h - q_h = C_h \frac{dT_{hf}}{dt} \qquad (10.1)$$

where, $\dot{Q}_h$ = power generated per ft^2 of surface area at hot spot,

q_h = heat flux at surface at hot spot,

C_h = fuel heat capacity at hot spot,

T_{hf} = fuel temperature at hot spot.

If the steam heat capacity is neglected with respect to C_h;

$$q_h = H_h(T_{hf} - T_{hs}) \qquad (10.2)$$

where, T_{hs} is the steam temperature at the hot spot.

The heat transfer coefficient "H_h" is considered as a function of steam flow only, so that:

$$H_h = H_{ho}(W_s/W_{so})^{0.8} \qquad (10.3)$$

If the neutron flux throughout the entire superheater is assumed to vary uniformly with the neutron flux calculated in Sec. 2; then,

$$\dot{Q}_h = n \frac{\dot{Q}_{ho}}{n_o} \tag{10.4}$$

and

$$W_s(h_h - h_1) = \frac{q_h}{\dot{Q}_{ho}} W_{so}(h_{ho} - h_{1o}) \tag{10.5}$$

Changes in the hot spot steam temperature are related to steam enthalpy changes simply by:

$$\delta T_{hs} = \frac{\delta h_h}{c_p} \tag{10.6}$$

since c_p, the specific heat of steam, is very nearly a constant in the lower regions of the superheater for all reasonable pressure and temperature swings. Because of assumption 1, the bulk steam temperature change at the superheater exit can be written as:

$$\delta T_2 = \delta T_{hs} \frac{c_p(h_{2o} - h_{1o})}{c_{p2}(h_{ho} - h_{1o})} \tag{10.7}$$

where, h_2 and c_{p2} are the enthalpy and specific heat of steam at the exit. The inlet enthalpy, h_1, is considered constant.

Because of the negligible steam heat capacity, the above set of equations must be re-arranged to avoid an algebraic loop in the analog simulation. If Eqs. 10.2, 10.3, 10.5 and 10.6 are combined to eliminate T_{hs}, h_h, and H_h, there results:

$$q_h = \left[\frac{H_{ho}(W_s/W_{so})^{0.8}}{1 + \frac{H_{ho}(h_{ho} - h_{1o})}{c_p \dot{Q}_{ho}} (W_s/W_{so})^{-0.2}}\right] \left[T_{hf} - T_{hso} + \frac{(h_{ho} - h_{1o})}{c_p}\right]. \tag{10.8}$$

When Eq. 10.8 is applied to the Pathfinder superheater hot spot, the first bracket is almost linear with steam flow rate between 0 and 110 per cent flow. Therefore, it is approximated by:

$$\frac{W_s}{W_{so}} \left[\frac{H_{ho}}{1 + \frac{H_{ho}(h_{ho} - h_{lo})}{c_p \dot{Q}_{ho}}} \right] \equiv H_h' \frac{W_s}{W_{so}} \qquad (10.9)$$

Using this approximation in Eq. 10.8 and keeping only the transient part of the results:

$$\delta q_h = H_h' \left[\delta T_{hf} + \frac{T_{hfo} - T_{hso} + \frac{h_{ho} - h_{lo}}{c_p}}{W_{so}} \delta W_s + \frac{\delta T_{hf} \, \delta W_s}{W_{so}} \right] \qquad (10.10)$$

Combining Eqs. 10.5, 10.6, and 10.8, the approximation of Eq. 10.9, and keeping only the transient parts:

$$\delta T_{hs} = \frac{H_h' (h_{ho} - h_{lo})}{c_p \dot{Q}_{ho}} \delta T_{hf} \qquad (10.11)$$

And, finally, combining the transient parts of Eqs. 10.1 and 10.4

$$\frac{\dot{Q}_{ho}}{n_o} \delta n - \delta q_h = C_h \frac{dT_{hf}}{dt} \qquad (10.12)$$

Eqs. 10.10, 10.11, 10.12, and 10.7 are simulated with δn and δW_s as the inputs and δT_s, δT_{hf}, δT_2, and δq_h as the available outputs.

11. THE STEAM SYSTEM

The equations describing the pertinent steam flows and pressures from the reactor dome through to the turbine and dump valve are derived here. The dynamic effect of steam compressibility is taken into account. These equations

generate the input (steam-line pressure) and use the output (turbine-inlet and dump-valve positions) of the control system (Sec. 12). The steam flow schematic is Figure 11.1.

Assumptions

1. The steam is sufficiently superheated to follow the perfect gas law.

2. The steam inertia can be neglected.

3. Shock wave phenomena are not considered.

Assumptions 2 and 3 have been analytically proved valid. Any shock waves set up in the line are highly damped.

Derivation

a) Steam Line Pressures

The superheater exit pressure variation is:

$$\delta P_2 = \delta P_1 - \Delta P_s + \Delta P_{so} \qquad (11.1)$$

(refer to Figure 11.1 for symbol definitions)

and at the turbine inlet:

$$\delta P_3 = \delta P_2 - \Delta P_{sl} + \Delta P_{slo} \qquad (11.2)$$

where, the superheater pressure drop (ΔP_s) is shown in Figure 11.2 as a function of steam flow rate. The steam line pressure drop is:

$$\Delta P_{sl} = (\Delta P_{slo}/W_{slo}^2)\, W_{sl}^2 \qquad (11.3)$$

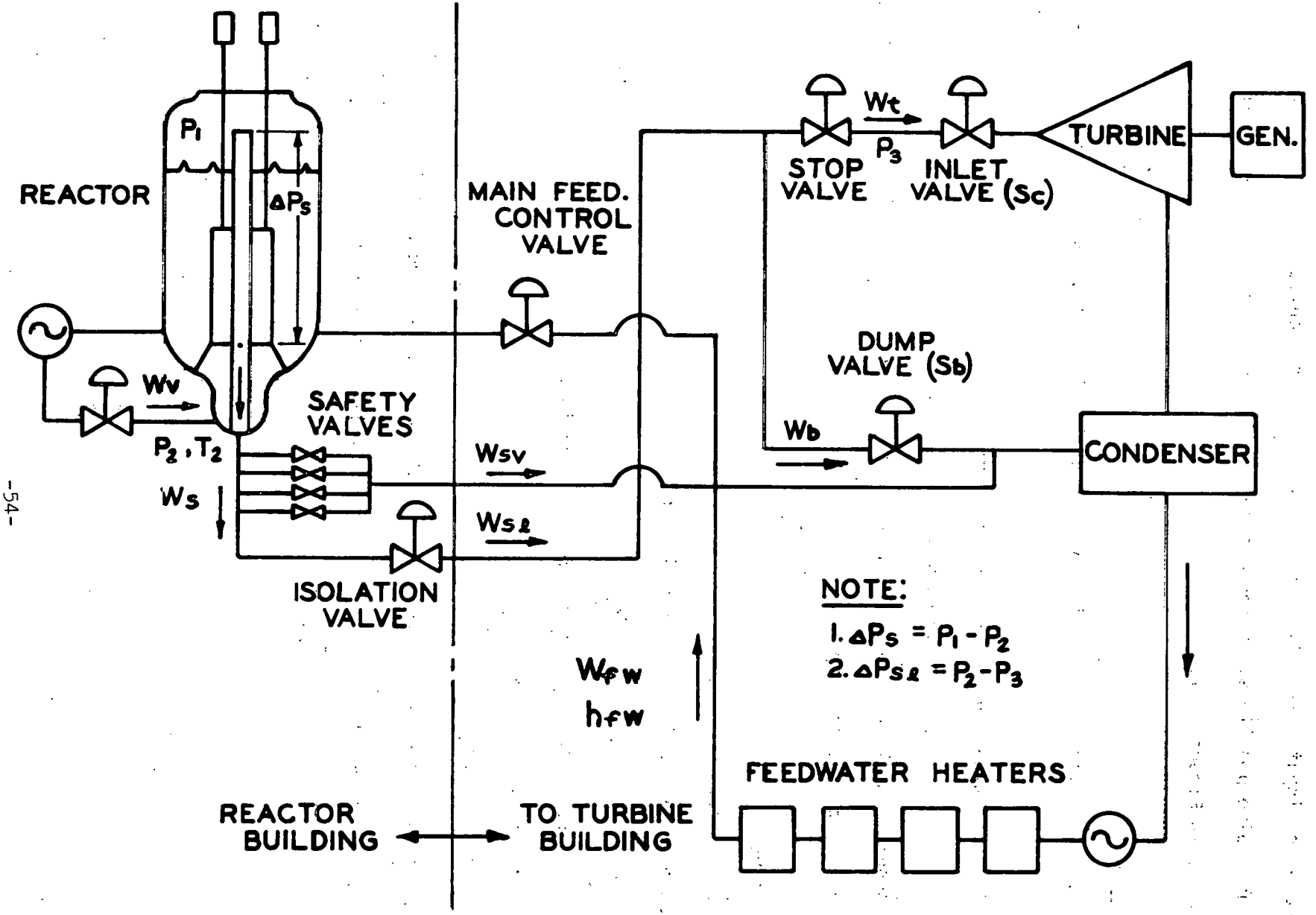

Figure II.1 Steam-flow schematic. (A-C Dwg. 43-024-804)

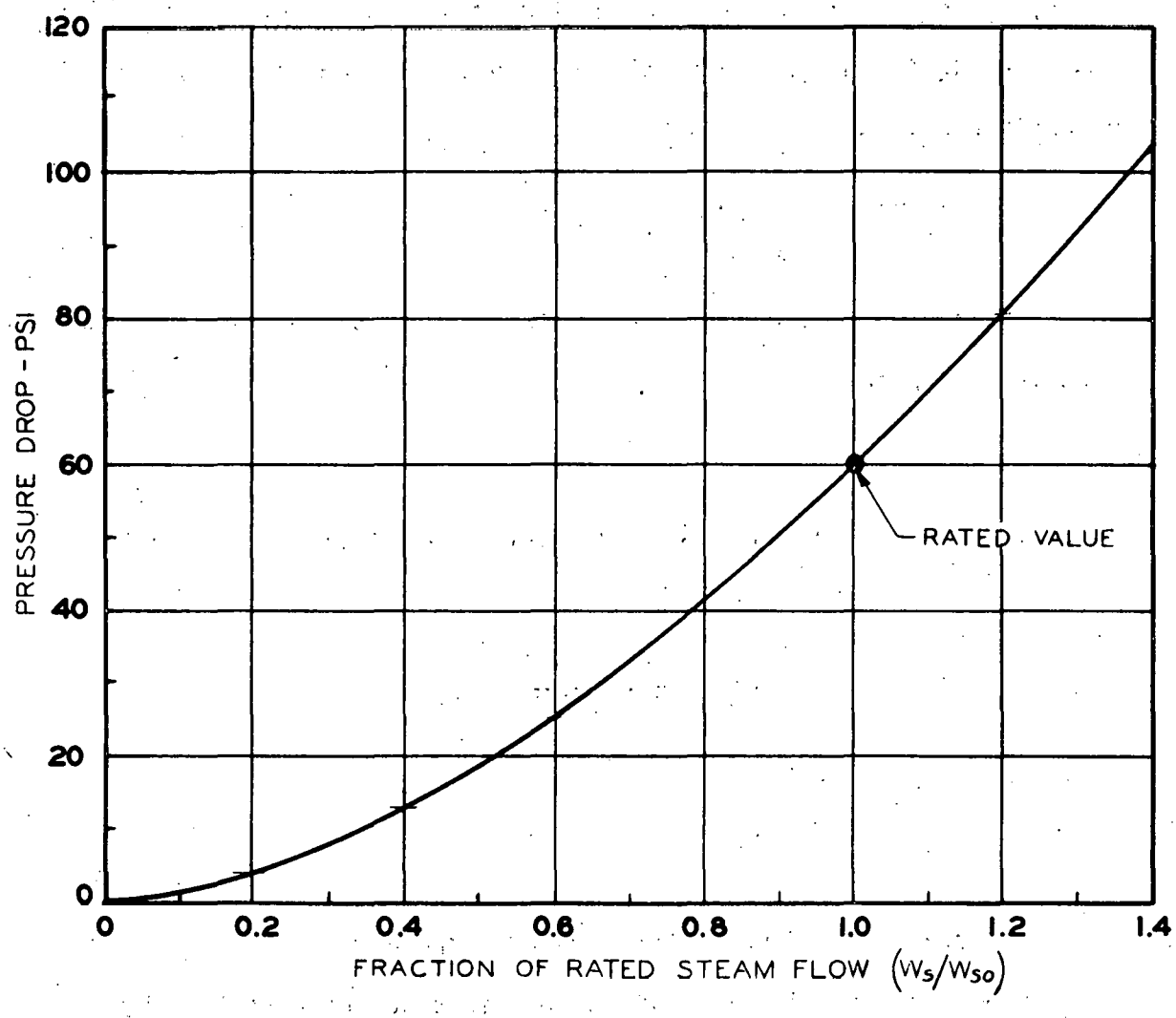

Figure 11.2 Superheater pressure drop versus steam flow.
(A-C Dwg. 43-024-763)

b) Steam Line Thermodynamics and Flow Balances

Using assumptions 1, 2 and 3, and using P_2 as the average steam line pressure (since ΔP_{sl} is small), the steam line thermodynamics can be described by the perfect gas law,

$$P_2 = R_s T_2 M_s / 144\ V_s \tag{11.4}$$

where, T_2, M_s and V_s are the temperature, mass and volume of the steam in the line, and R_s is the gas constant for steam. T_2 here is degrees Rankine. A reversible adiabatic process is assumed,

$$T_2 P_2^{\frac{1-k}{k}} = T_{2o} P_{2o}^{\frac{1-k}{k}} \tag{11.5}$$

where, k is the ratio of specific heats for the superheated steam and the steam line mass balance:

$$\frac{dM_s}{dt} = \delta W_{sl} - \delta W_t - \delta W_b \tag{11.6}$$

Linearizing Eq. 11.4 and 11.5, and solving Eqs. 11.4, 11.5, and 11.6 to eliminate T_2 and M_s:

$$\delta W_{sl} = \delta W_t + \delta W_b + \frac{144\ V_s}{k R_s T_{2o}} \frac{dP_2}{dt} \tag{11.7}$$

Also, from Figure 11.1:

$$\delta W_s = \delta W_{sl} + \delta W_{sv} \tag{11.8}$$

c) Steam Flow Through Turbine and Dump Valve

Flow through the turbine is critical and thus can be described by

$$W_t = S_c P_3 / \sqrt{P_3 V_s} \tag{11.9}$$

where S_c, the "capacity coefficient", is proportional to the inlet valve position. The product of the pressure and specific volume (P_3v_s) is considered constant.

Flow through the dump valve may be similarly described by

$$W_b = S_b P_3 / \sqrt{P_3 v_s} \qquad (11.10)$$

where, S_b, the "capacity coefficient", is proportional to valve position.

The transient parts of Eqs. 11.9 and 11.10 are:

$$\delta W_t = (1/\sqrt{P_3 v_s})(S_{co}\delta P_3 + P_{3o}\delta S_c + \delta P_3 \delta S_c) \qquad (11.11)$$

and

$$\delta W_b = (1/\sqrt{P_3 v_s})(P_{3o}\delta S_c + \delta P_3 \delta S_c). \qquad (11.12)$$

Eqs. 11.2, 11.3, 11.4, 11.5, 11.7, 11.8, 11.11, and 11.12 are simulated using the values listed in the symbol sheets for the constants.

d) Reactor Safety Valves

Four safety valves are located at the superheater exit and will pass steam directly to the condenser. Figure 11.3 shows the individual capacities of the four valves for both increasing and decreasing pressure at the valves. The fourth safety valve is a dual purpose valve which operates automatically on overpressure or by motor drive on simultaneous closure of turbine and dump valves.

The pair of general equations describing the flow through each safety valve after P_2 has reached the relief pressure, and before it drops below the reset pressure are:

$$\begin{aligned} (W_{sv})_i &= m_i P_2 - b_i \quad , \quad P_{ri} \leq P_2 \leq P_{pi} \\ &= (m_i - m_{ii})\, P_2 + b_{ii} - b_i \quad , \quad P_2 > P_{pi} \end{aligned} \qquad (11.13)$$

where the subscript "i" indicates the safety valve number, and P_{ri} and P_{pi} are

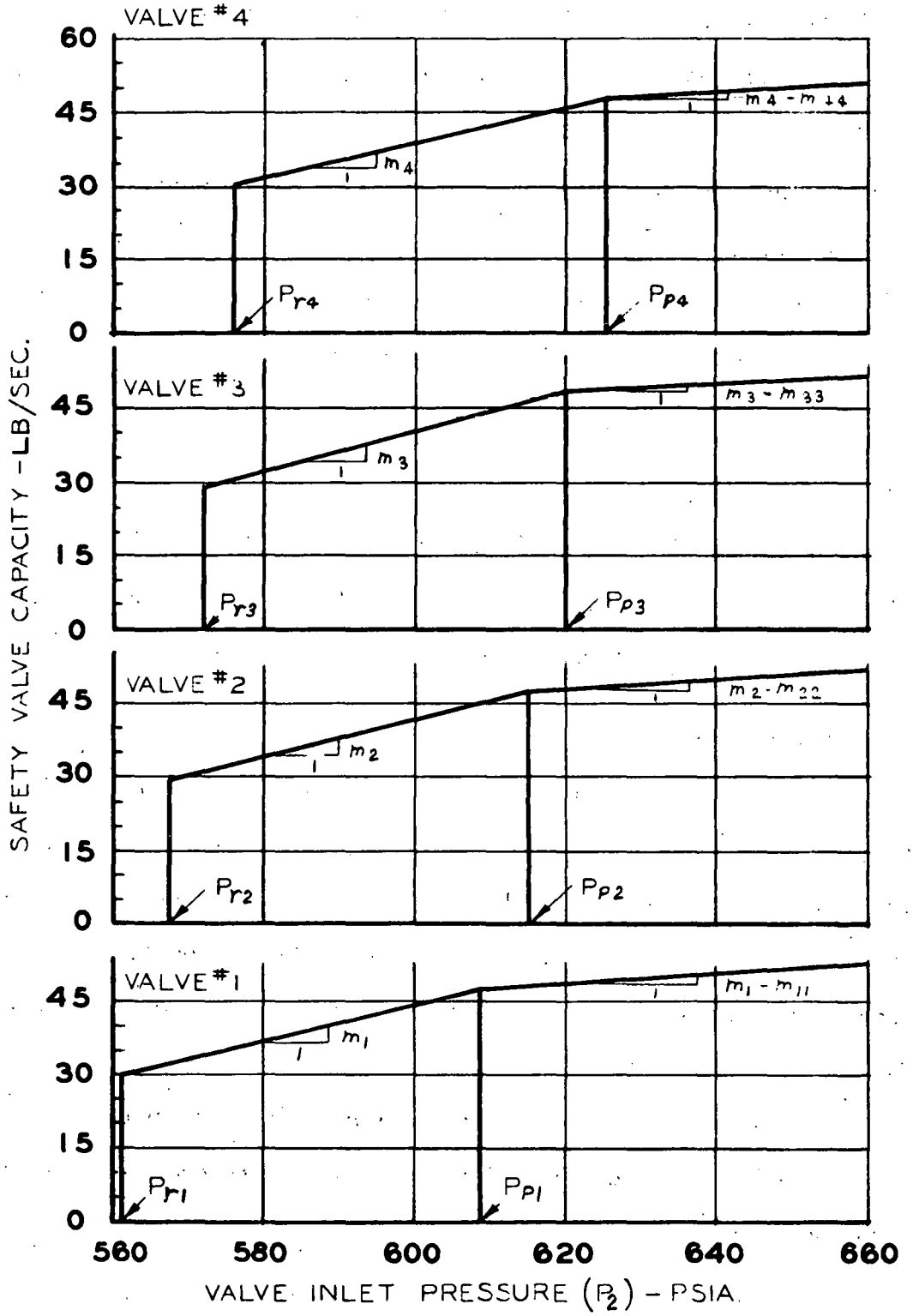

Figure 11.3 Individual safety valve characteristics.
(A-C Dwg. 43-024-765)

reset and popping pressures, respectively. It is assumed that each valve has the same simple lag response for opening and closing. Thus;

$$W_{sv} = \frac{\sum_{i=1}^{4} (W_{sv})_i}{1 + \tau_{sv} s} \qquad (11.14)$$

12. ACTUATORS AND CONTROLS FOR THE TURBINE INLET AND DUMP VALVES

The functional schematic of the controls is shown in Figure 12.1. The turbine inlet valve is positioned by steam-line pressure error through a triple-action controller (RP-10a). The pressure set-point is modified during transients by a temperature error signal from the superheater exit steam, in order to minimize superheater temperature transients. The temperature error signal is first sent through a proportional-plus-rate controller to compensate for its measuring lag. The dump valve opens, and assumes the pressure regulation, only if the turbine inlet valves have reached their fully open position. The "excess demand" signal reaches the dump valve actuator through summer RP-10e.

For emergency conditions such as turbine trip or load dump, a relay system is provided to quickly open the dump valve. The simulation of this relay system will be included in a subsequent report because it is considered as a special input to the basic simulator.

Assumptions

1. Velocity limiter RP-10d perfectly matches the dynamics of the inlet valve and actuator.

2. The measuring lag of temperature transducer 960 varies as the inverse of steam flow to the 0.8 power.

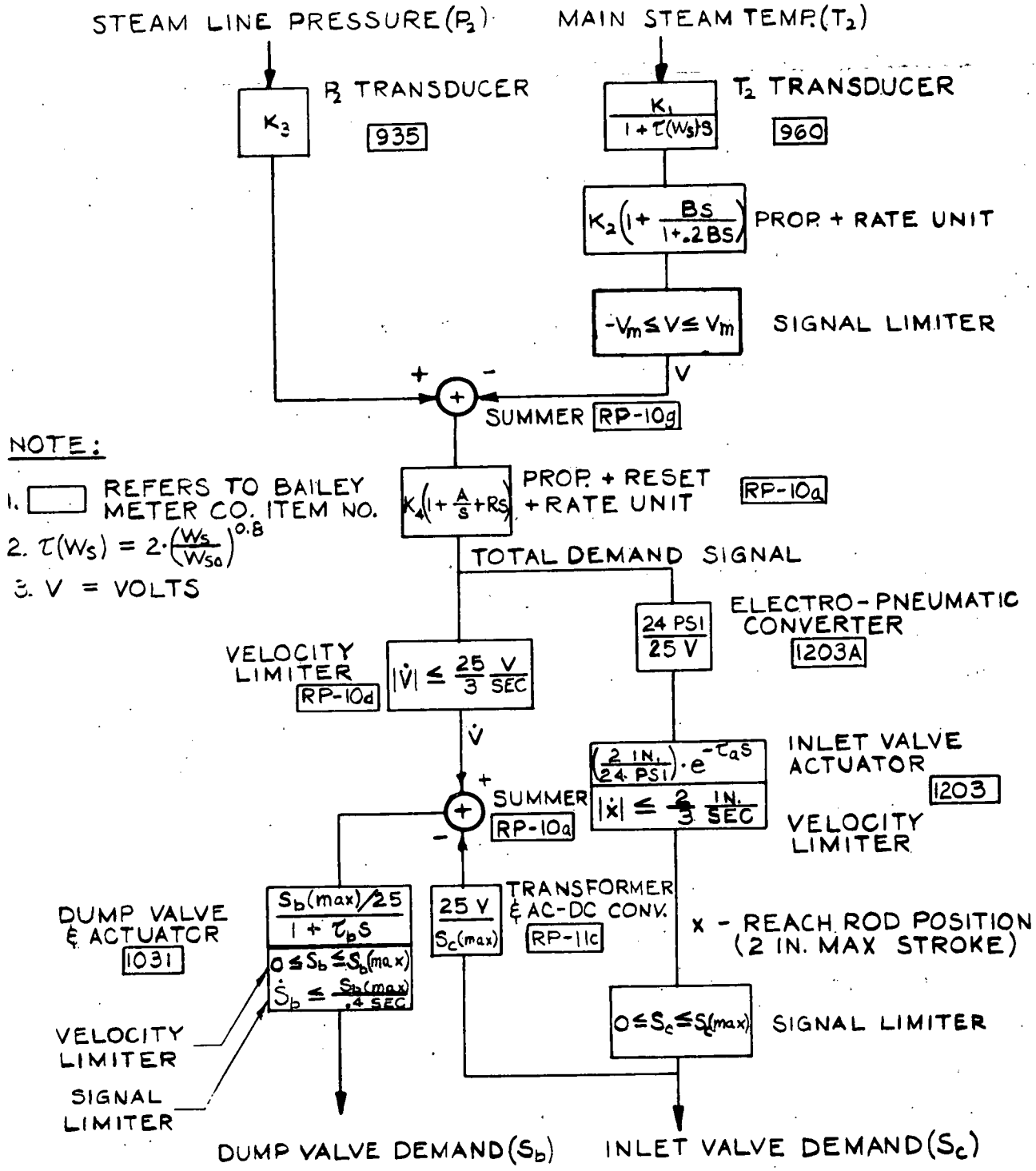

Figure 12.1 Pressure control system functional diagram.
(A-C Dwg. 43-024-767)

Derivation

a) Turbine Inlet Valves Actuator

A pneumatic actuator moves a "reach rod" into the hydraulic turbine control system. This hydraulic system consists of a pilot valve, a power piston and cylinder, and mechanical linkages. The experimental dynamic response of the pneumatic actuator alone approximates a perfect lag of τ_a sec, and is simulated as such (Figure 15.14). The response of the hydraulic system was calculated as an order of magnitude faster, so it is assumed instantaneous on the simulator.

The pneumatic actuator can move the valve at a rate no faster than full travel in 3 sec. This limit, along with the fully open and fully closed limits for valve travel, are included in the simulation.

b) Dump Valve Actuator

Experimental response data for the hydraulic dump valve actuator has not been available. A simple lag of τ_b sec. is assumed, since the response should be quite fast anyway. The minimum opening time for the valve is 0.4 sec. This limit, along with the fully open and fully closed limits for valve travel, are included in the simulation.

c) Controls

The lags due to pneumatic tubing, response of the pressure transducer, etc., were found to be so short that they can be neglected with respect to the cut-off frequency of the pneumatic actuator. As mentioned in assumption 1, the two inputs of summer RP-10e exactly cancel each other unless the inlet valves are fully open, in which case the demand signal actuates the dump valve.

The actions of the rest of the control components are obvious from Figure 12.1.

13. FEEDWATER SYSTEM

The feedwater flow is regulated by the reactor level control system, which insures that the feedwater flow is always proportional to the steam flow. The feedwater is heated by turbine bleed steam in the feedwater heaters, so its temperature varies with steam flow. A regulating system is included in the last heater to prevent the final feedwater temperature from dropping below 340 F. Thus, above 81 per cent steam flow, the feedwater temperature increases with steam flow, and below 81 per cent it remains at 340 F.

Assumptions

1. The level control system is represented by a simple lag by which changes in feedwater flow lag changes in steam flow.

2. Feedwater enthalpy is linear with steam flow at steam flows above 81 per cent rated, and constant at 311.1 Btu/lb below this point.

Derivation

a) Feedwater Flow

The transfer function of the level control system and feedwater valve actuator is assumed to be a simple lag:

$$\delta W_{fw} = \frac{\delta W_s}{1 + \tau_{fv} s} \qquad (13.1)$$

where, W_{fw} and W_s are the feedwater and steam flows, respectively, and τ_{fv} is estimated at about 2 sec.

b) Feedwater Temperature

Between 81 and 100 per cent steam flow, the feedwater enthalpy changes at a rate of about 0.54 Btu/lb per lb/sec of steam flow. Below 81 per cent steam flow, the regulating system keeps it constant at 311.1 Btu/lb, or 94.6 per cent of its rated value. The time constant due to transport lag through the feedwater heaters at rated flow is estimated at about 20 sec. (τ_{fh}). The equations describing this system are:

$$\delta h_{fw} = \frac{\partial h_{fw}}{\partial W_s} \frac{1}{1 + \tau_{fh} s} \qquad \delta W_s > -19\% \; W_{so}$$

$$\delta h_{fw} = -5.4\% \; h_{fwo} \qquad \delta W_s < -19\% \; W_{so} \tag{13.2}$$

14. RECIRCULATION FLOW HYDRODYNAMICS

The study of the hydrodynamics of the recirculation system is broken down into three areas:

1. Inter-loop flow of the three recirculation loops:

The individual flow rates can be expected to be very similar in the operating recirculation loops if the butterfly valves are operated in a ganged manner, since the core head loss (common to all loops) is quite large as compared with the individual loop head losses. The individual losses are very nearly equal. Therefore, for simulation purposes the three loops are considered as one with the combined characteristics.

2. Flow division among the fuel channels:

Flow in individual or multiple-channel cores of the Pathfinder type with

forced recirculation is very stable. This permits consideration of the boiler core, for simulation purposes, as a single channel model with its parameters expressed as the radial averages.

3. Effect of core voids on recirculation flow rate:

Increased voids in the core can either increase or decrease the recirculation rate, depending on the magnitude of the flow rate and the operating mode of the recirculation loops. For natural circulation, an increase in voids increases the density change through the core and can increase the flow rate. At high recirculation flows, the "choking" effect presented by the voids overrides this density effect, and decreases the flow rate. During forced circulation, increased voids decreases the recirculation flow rate. The relation between core steam flow rate and recirculation flow rate due to these effects is derived in this section. The lower limit of the Pathfinder flow range is still high enough to have a negative void - recirculation flow coefficient.

Assumptions

1. The dynamic effect of the water inertia during flow changes is neglected. The inertia of the pump impellers need not be included because they run at essentially constant speed.

2. The approximation shown on Figure 14.1 is made.

Derivation

Characteristic curves of core steam flow versus recirculation flow were calculated for several butterfly valve positions for one, two, and three pump operation. These characteristics are fairly linear, and their slopes $\partial W_v/\partial W_{fg}$

are plotted against their zero steam flow intercepts (W'_v) in Figure 14.1. The "linear approximation" of Figure 14.1 is used in the simulation.

The approximate equation of Figure 14.1 is integrated, and the boundary conditions

$$W_v = W'_v \text{ at } W_{fg} = 0$$

and

$$W_v\ W_{vo},\ W'_v\ W'_{vo} \text{ at } W_{fg} = W_{fgo}$$

are applied. The transient part of the result is:

$$\delta W_v = \delta W_{fg} \left(\frac{1.1 - 4.8 \times 10^{-4} W_{vo}}{1 - 4.8 \times 10^{-4} W_{fgo}} \right) + \delta W'_v \left(1 - 4.8^{-4} W_{fgo} \right) - 4.8 \times 10^{-4}\ \delta W_{fg}\ \delta W'_v \qquad (14.1)$$

where, W'_v is a function of pump speed and butterfly valve position.

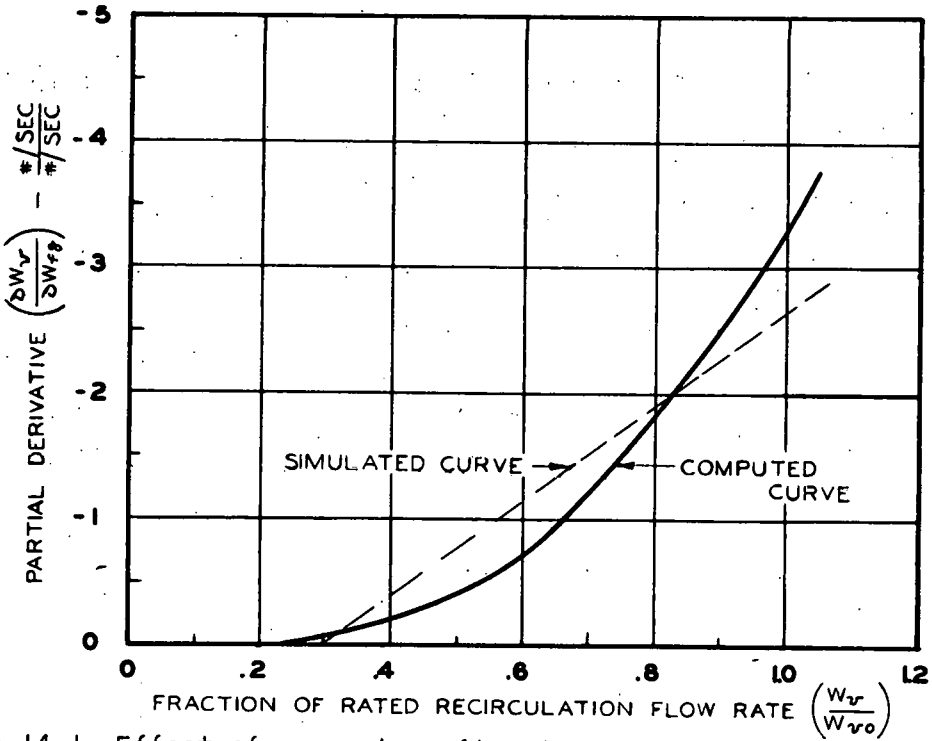

Figure 14.1 Effect of core steam flow (W_{fg}) on recirculation flow rate (W_v). (A-C Dwg. 43-024-766)

15. ELECTRONIC ANALOG COMPUTER SIMULATION

15.1 Introduction

This section gathers the final equations from the other sections and shows the computer circuitry used to simulate the equations. The subsections herein are numbered in accordance with the previous sections; for example, the equations and circuitry for Sec. 2, "Neutron Kinetics", are contained in Sec. 15.2 In some instances rearrangement and combination of the equations developed in the preceding sections, as well as some additional equations, are necessary for the computer model.

The pot settings are shown on the diagrams where it is convenient. However, all pot settings are given both symbolically and numerically in Appendix A. All symbols appearing here and in Appendix A are defined, given units, and evaluated in Appendix B.

Several circuits, such as those simulating control rod motion, scram, turbine trip, etc., are not shown here because they are classified as special inputs to the basic simulator, and, hence, beyond the scope of this report.

The circuitry used is drawn in symbolic form showing the actual computer components utilized. The definitions of the computer symbols used in these diagrams are given in Figure 15.18, and the complete computer diagram of the system is shown in Figure 15.19.

15.2 Simulation of the Neutron Kinetics

The equation generating change in neutron population is

$$\frac{dn}{dt} = \frac{(\delta k_{ex} - 1)\, n}{l^*/\beta} + \sum_{i=1}^{6} \lambda_i C_i \qquad (15.1)$$

where each of the six groups of delayed neutrons are from

$$\frac{dC_i}{dt} = \frac{\beta_i n}{l^*} - \lambda_i C_i \qquad (15.2)$$

and the excess reactivity is generated by

$$\delta k_{ex} = k_{rods} - k_v - k_d \qquad (15.3)$$

The analog circuitry for these eight equations is shown on Figure 15.1.

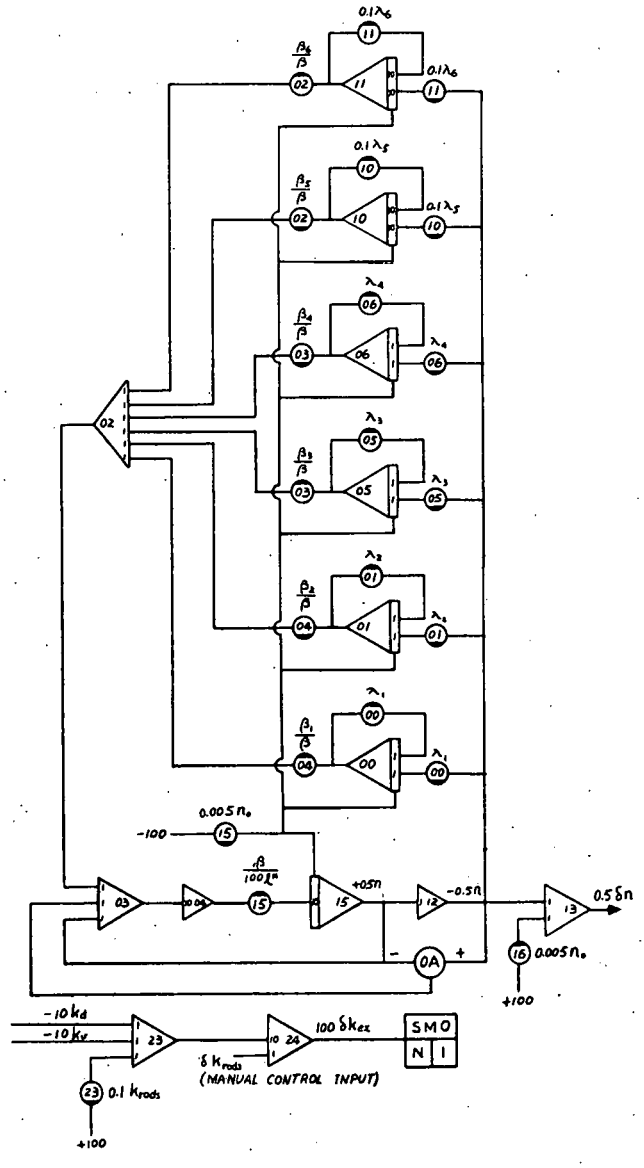

Figure 15.1 Computer diagram for neutron kinetics.

15.3 Simulation of Boiler Fuel Heat Transfer

Combining Eqs. 3.13 and 3.14, there results:

$$\frac{\dot{Q}_b(s)}{n_i(s)} = \frac{\dot{Q}_{go}}{n_o}(1-\gamma)\left[\sum_{i=1}^{3}\frac{F_i}{1+\tau_i s} + \frac{1-\sum_{i=1}^{3}F_i}{1+\tau_4 s}\right] + \frac{Q_{go}\,\gamma}{n_o} \qquad (15.4)$$

which is simulated by the circuit shown in Figure 15.2.

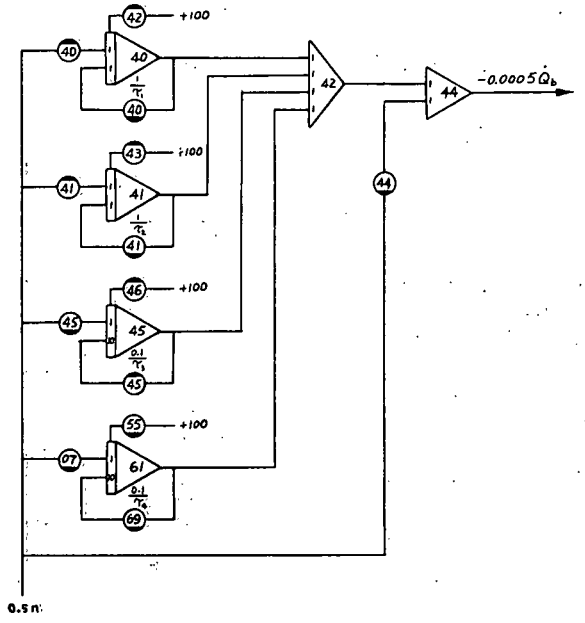

Figure 15.2 Computer diagram for boiler heat transfer

15.4 Simulation of the Doppler Effect

A fraction, γ, of the heat generated is transferred immediately by nuclear radiation to the coolant, hence, it has no effect on fuel temperature. Using this fact, and combining Eqs. 3.14 and 4.3, the reactivity due to fuel temperature change is:

$$k_d = \frac{\partial k_d}{\partial T_{avg}} \frac{1}{C} \int_o^t \left[(1-\gamma) \frac{\dot{Q}_{go}}{n_o} n - (Q_b - \gamma \frac{\dot{Q}_{go}}{n_o} n) \right] dt \qquad (15.5)$$

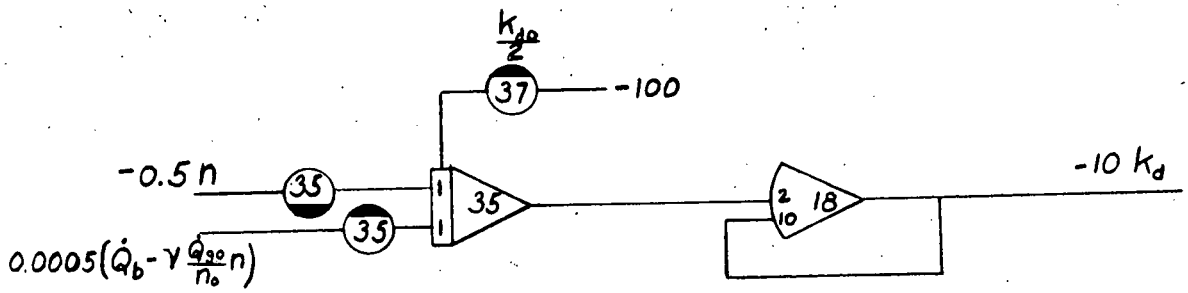

Figure 15.3 Computer diagram for Doppler reactivity.

15.5 Simulation of the Energy, Mass, and Volume Balance of Saturated Part of Primary System

If the denominator of Eq. 5.6 is defined as "D", and the following substitutions are made in Eq. 5.6:

$$\dot{Q}_m = \frac{\dot{Q}_{mo}}{n_o} n \tag{15.6}$$

$$W_s = \delta W_s + W_{so} \tag{15.7}$$

$$W_{fw} = \delta W_{fw} + W_{fwo} \tag{15.8}$$

there results:

$$\frac{dP_1}{dt} = \frac{1}{D}\left\{\dot{Q}_b + \frac{\dot{Q}_{mo}}{n_o} n - W_v \Delta h + \frac{h_{fg} v_f}{v_{fg}} \delta W_{fw} - \left(1 + \frac{v_f}{v_{fg}}\right) h_{fg}\, \delta W_s \right.$$

$$\left. - \left[\left(1 + \frac{v_f}{v_{fg}}\right) h_{fg}\, W_{so} - \frac{h_{fg} v_f}{v_{fg}} W_{fwo} - W_{ps} + W_p\right]\right\} \tag{15.9}$$

where the terms in the brackets are constant.

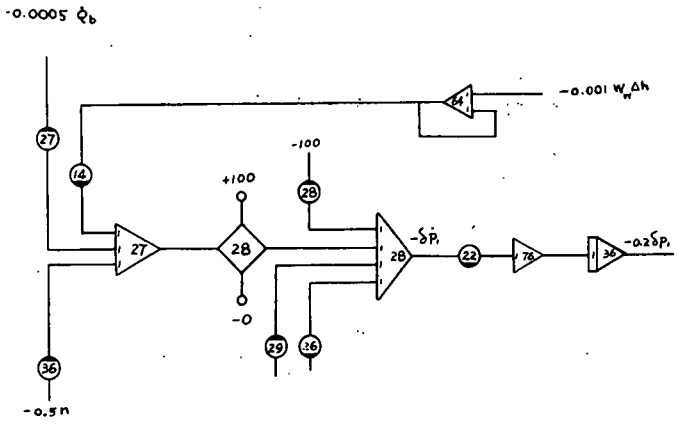

Figure 15.4 Computer diagram for generation of reactor pressure.

15.6 Simulation of the Energy and Mass Balances of the Subcooled Part of the Primary System.

Eqs. 6.6, 6.7 and 6.8 are combined with the relations

$$\delta h_f = \frac{\partial h_f}{\partial P_l} \delta P_l \tag{15.10}$$

and

$$\delta W_r \delta h_r \simeq (\delta h_f - \delta \Delta h)\ \delta W_r \tag{15.11}$$

to obtain:

$$W_v \cdot \Delta h = W_{ro} \left(\frac{\partial h_f}{\partial P_l} \quad \frac{1}{\rho J} \right) \delta P_l + \Delta h_o \delta W_r - W_{po} \Delta h$$

$$+ \delta W_r \delta \Delta h + W_{ro} \Delta h_o$$

$$- \left\{ \left[W_{ro} \left(1 - \frac{1}{\rho J \partial h_f / \partial P_l} \right) - W_{fwo} \right] \frac{\partial h_f}{\partial P_l} \delta P_l + (h_{fo} - h_{ro})\ \delta W_r \right.$$

$$+ (\delta W_r - \delta W_{fw}) \frac{\partial h_f}{\partial P_l} \delta P_l - (h_{fo} - h_{fwo})\ \delta W_{fw}$$

$$\left. + \delta W_{fw} \delta h_{fw} + W_{fwo} \delta h_{fw} + \delta W_r \left(\delta \Delta h - \frac{\partial h_f}{\partial P_l} \delta P_l \right) \right\} \epsilon^{-T_r s} \tag{15.12}$$

where the steady state value of Δh is evaluated from Eq. 6.9.

The computer diagram of Eq. 15.12 is shown in Figure 15.6.

The analog simulation of transport delay is approximated by the following transfer function.

$$\epsilon^{-T_r s} \approx \frac{476 - 160.5\ T_r s + 22.8\ T_r{}^2 s^2 - 1.48\ T_r{}^3 s^3}{476 + 309\ T_r s + 91.8\ T_r{}^2 s^2 + 12.1\ T_r{}^3 s^3 + T_r{}^4 s^4} \tag{15.13}$$

which is preferable if the signal to be delayed contained frequencies about $\omega = \frac{4}{Tr}$, as in step response or ramp response. (The transport delay circuit is shown in Figure 15.5.)

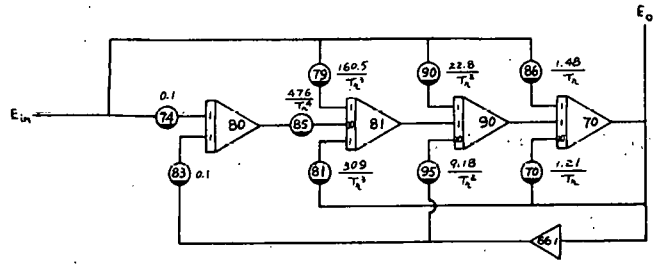

Figure 15.5 Computer diagram for transport delay circuit.

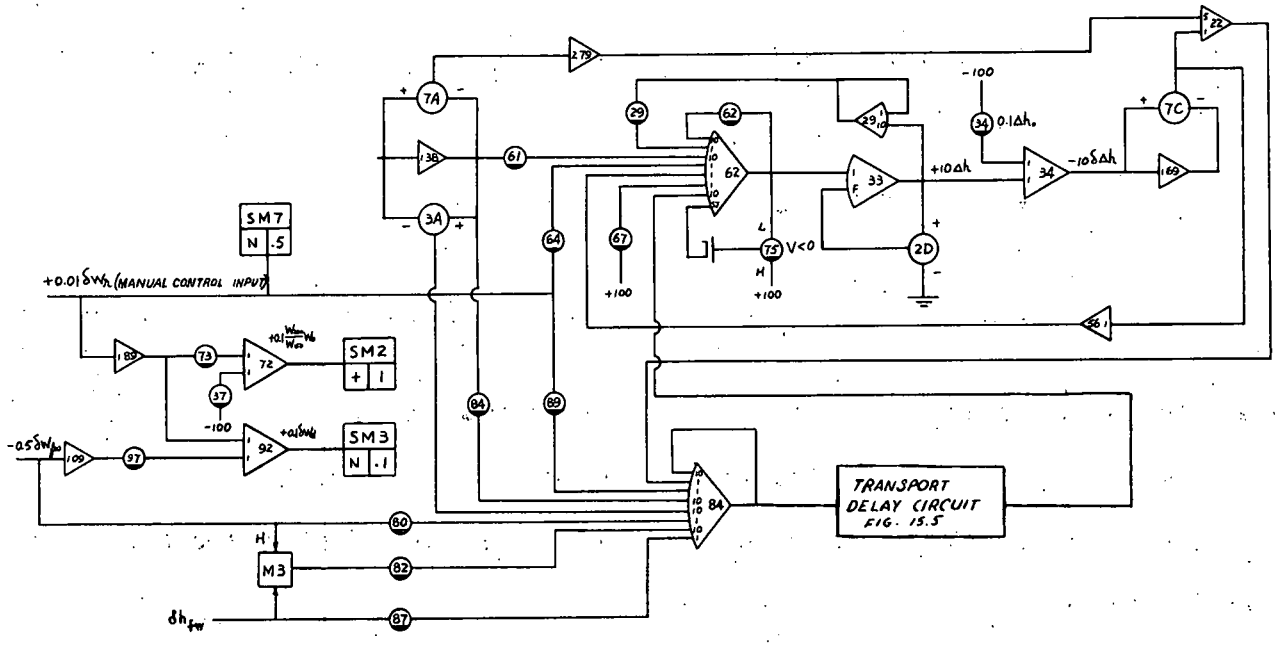

Figure 15.6 Computer diagram for generation of subcooling.

15.7 Simulation of the Reactivity in Voids

The reactivity in voids is simulated by the following relations

$$k_v = \frac{\partial k_v}{\partial \bar{\alpha}} F(\bar{x}) \qquad (15.14)$$

$$\bar{x} = I\, x_e - E\frac{\Delta h}{h_{fg}} \qquad (15.15)$$

$$x_e = W_{fg}/W_w \qquad (15.16)$$

$$W_{fg} = \frac{\dot{Q}_b}{h_{fg}} - \frac{\Delta h W_w}{h_{fg}} - \frac{\partial W_{fg}}{\partial P_1}\dot{P}_1 \qquad (15.17)$$

$$W_w = \frac{W_{wo}}{W_{vo}} W_v \qquad (15.18)$$

The computer circuitry is shown in Figure 15.7. Since x_e and $\bar{x}$ have to be positive values, a bridge limiter is used between amplifiers 39 and 32 and a diode limiter is used on amplifier 19. The function is scaled such that the voltages of both the input and output signals are around 50 v at 100 per cent power.

The function generator F_60 generates the steam volume-weight correlation shown in Figure 7.1.

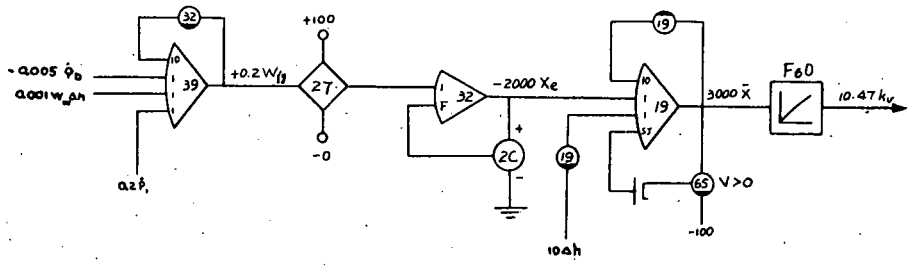

Figure 15.7 Computer diagram for void reactivity

15.8 Simulation of the Void Redistribution Dynamics

A good enough approximation to the void redistribution transfer function is a simple lag with time constant τ_v.

$$g(s) = 1/(1 + \tau_v s) \qquad (15.19)$$

It requires only one integrator as shown in Figure 15.8.

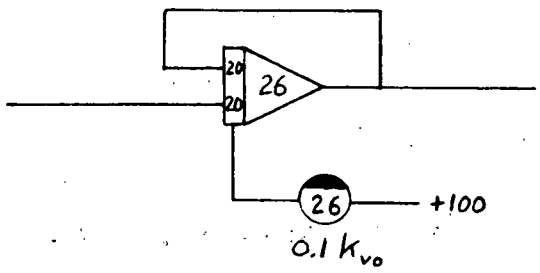

Figure 15.8 Computer diagram for void redistribution.

15.9 Simulation of Static Pressure Effect on Reactivity.

Substituting $k_v \frac{\partial \bar{\alpha}}{\partial k_v}$ for $\bar{\alpha}$ in Eq. 9.6 and re-arranging the results:

$$\delta k_v = - \delta P_1 (1 - \bar{\alpha}) \left[\frac{\partial k_v}{\partial \bar{\alpha}} \frac{1}{v_f} \frac{\partial v_f}{\partial P_1} + k_v \left(\frac{1}{v_g} \frac{\partial v_g}{\partial P_1} - \frac{1}{h_{fg}} \frac{\partial h_{fg}}{\partial P_1} - \frac{1}{v_f} \frac{\partial v_f}{\partial P_1} \right) \right] \quad (15.20)$$

where the factor $(1 - \bar{\alpha})$ is considered constant to simplify the simulation.

The simulation is shown in Figure 15.9.

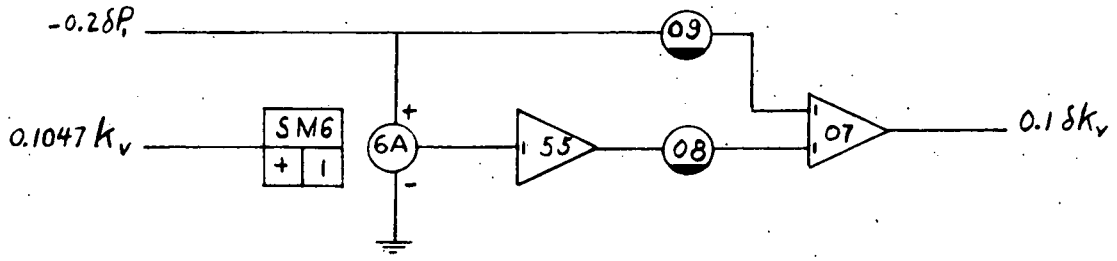

Figure 15.9 Computer diagram for static pressure reactivity.

15.10 Simulation of Superheater Temperatures.

Eqs. 10.10 and 10.12 are combined to give

$$\frac{dT_{hf}}{dt} = \frac{1}{C_h}\left[\frac{\dot{Q}_{ho}}{n_o}\delta n - H_h'\delta T_{hf} - H'\left(T_{hfo} - T_{hso} + \frac{h_{ho}-h_{10}}{C_p}\right)\frac{\delta W_s}{W_{so}} - H_h'\delta T_{hf}\frac{\delta W_s}{W_{so}}\right] \quad (15.21)$$

Eq. 10.11 is repeated here;

$$\delta T_{hs} = H_h'\frac{(h_{ho} - h_{10})}{C_p\,\dot{Q}_{ho}}\delta T_{hf} \quad (15.22)$$

And this, combined with Eq. 10.7, gives:

$$\delta T_2 = H_h'\frac{(h_{20} - h_{10})}{C_{p2}\,\dot{Q}_{ho}}\delta T_{hf} \quad (15.23)$$

Eqs. 15.21, 15.22, and 15.23 are simulated in Figure 15.10.

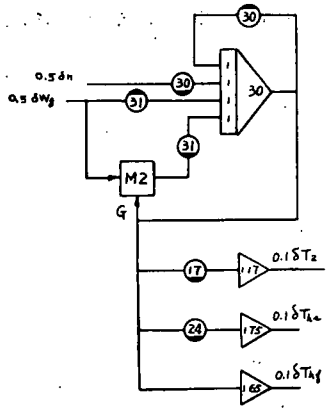

Figure 15.10 Computer diagram for superheater temperatures.

15.11 Simulation of the Steam System.

The equations used for simulating the steam system are the following:

$$\delta P_2 = \delta P_1 - \Delta P_s + \Delta P_{so} \tag{15.24}$$

$$\delta P_3 = \delta P_2 - \Delta P_{s1} + \Delta P_{s1o} \tag{15.25}$$

$$\Delta P_s = F(W_s) \tag{15.26}$$

$$\Delta P_{s1} = \frac{\Delta P_{s1o}}{W_{s1o}^2} W_{s1}^2 \tag{15.27}$$

$$\delta W_{s1} = \delta W_t + \delta W_b + \frac{144\ V_s}{kR_s\ T_{20}} \frac{dP_2}{dt} \tag{15.28}$$

$$\delta W_s = \delta W_{s1} + \delta W_{sv} \tag{15.29}$$

$$\delta W_t = (1/\sqrt{P_3 v_s})(S_{co}\delta P_3 + P_{30}\delta S_c + \delta P_3 \delta S_c) \tag{15.30}$$

$$\delta W_b = (1/\sqrt{P_3 v_s})(P_{30}\delta S_b + \delta P_3 \delta S_b) \tag{15.31}$$

$$(W_{sv})_i = m_i P_2 - b_i \quad , \quad P_{ri} \leq P_2 \leq P_{pi} \tag{15.32}$$

$$(W_{sv})_i = (m_i - m_{ii})P_2 + b_{ii} - b_i \quad , \quad P_2 \geq P_{pi} \tag{15.33}$$

$$W_{sv} = \frac{\sum_{i=1}^{3} (W_{sv})_i}{1 + \tau_{sv} s} \tag{15.34}$$

The computer circuitry is shown in Figure 15.11.

The feedback capacitor on amplifier 30 is used to break the algebraic loop in the superheater exit pressure circuit. The differentiating circuit is approximated by the following transfer function

$$\frac{E_o}{E_i} = \frac{s}{1 + (1-a)s} \tag{15.35}$$

where the constant "a" is set slightly less than 1.0.

The safety valves are simulated by using two relays for each valve as shown in Figure 15.12. When $P_2 \geq P_{pi}$ both relays operate, which gives the results shown in Eq. 15.33, when P_2 is reduced into the pressure range P_{pi} to P_{ri}, MO will keep operate but MI will reset, which gives the results shown in Eq. 15.32, and when $P_2 < P_{ri}$ both relays reset that means the safety valve is closed. There are three circuits of the form shown in Figure 15.12 simulating safety values No. 1, 2, and 3.

The function generated by F_7O is that shown on Figure 11.2.

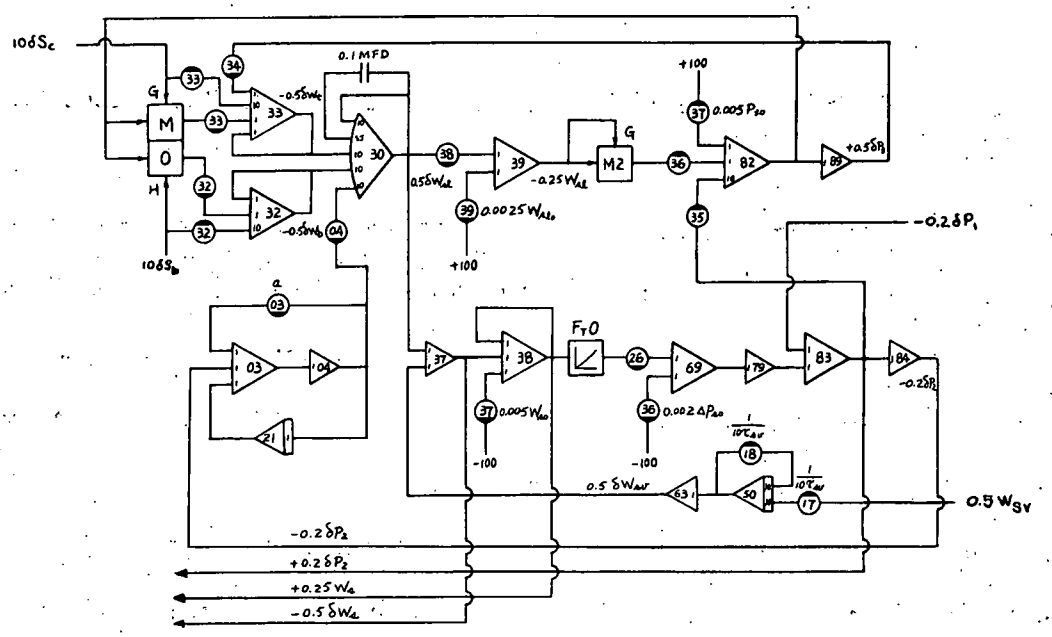

Figure 15.11 Computer diagram for steam system.

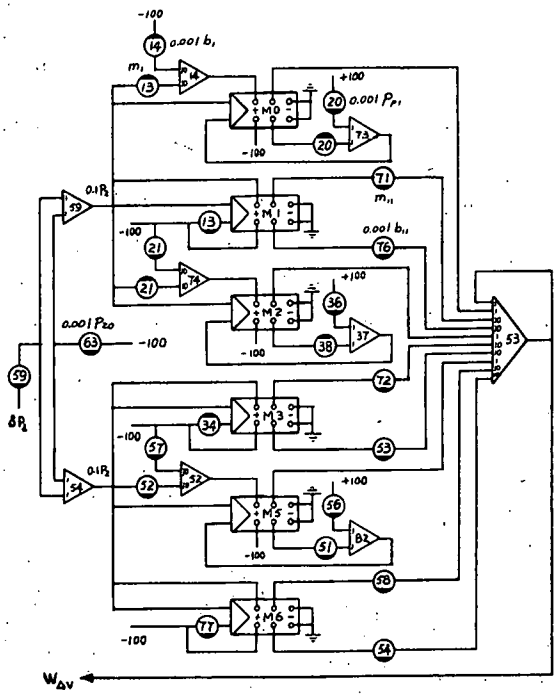

Figure 15.12 Computer diagram for safety valves.

15.12 Simulation of the Actuators and Controls for the Turbine Inlet and Dump Valves.

Figure 15.13 is the analog circuitry simulating the block diagram shown on Figure 12.1. Function generator F62 and the circuit of amplifier 00 simulate the variable lag of the T_2 transmitter, and amplifiers 01 and 02 simulate the proportional-plus-rate unit. Summer RP-10g is amplifier 12. The proportional-plus-reset-plus-rate unit is represented by amplifiers 11, 13, 26, 65, and 66 such that each of its three actions can be changed individually with a pot setting. Velocity limiter RP-10d and the rate of change limit of the inlet valve positioner both have a minimum time for full range changes of three seconds, hence can both be represented by the same circuit (amplifier 20).

The lag of the inlet valve positioner, τ_a, is represented by the same approximation as that used for the transport lag in Figure 15.6, except that τ_a is used instead of T_r. The comparison of the response of this circuit with that of the actual, experimental positioner response is shown in Figure 15.14. Amplifiers 31, 36, 90, 71, 75, and 19 form this circuit. Summer RP-10e is amplifier 23, and the circuit of amplifier 25 represents the 0.4 second close-to-open limit of the dump valve actuator.

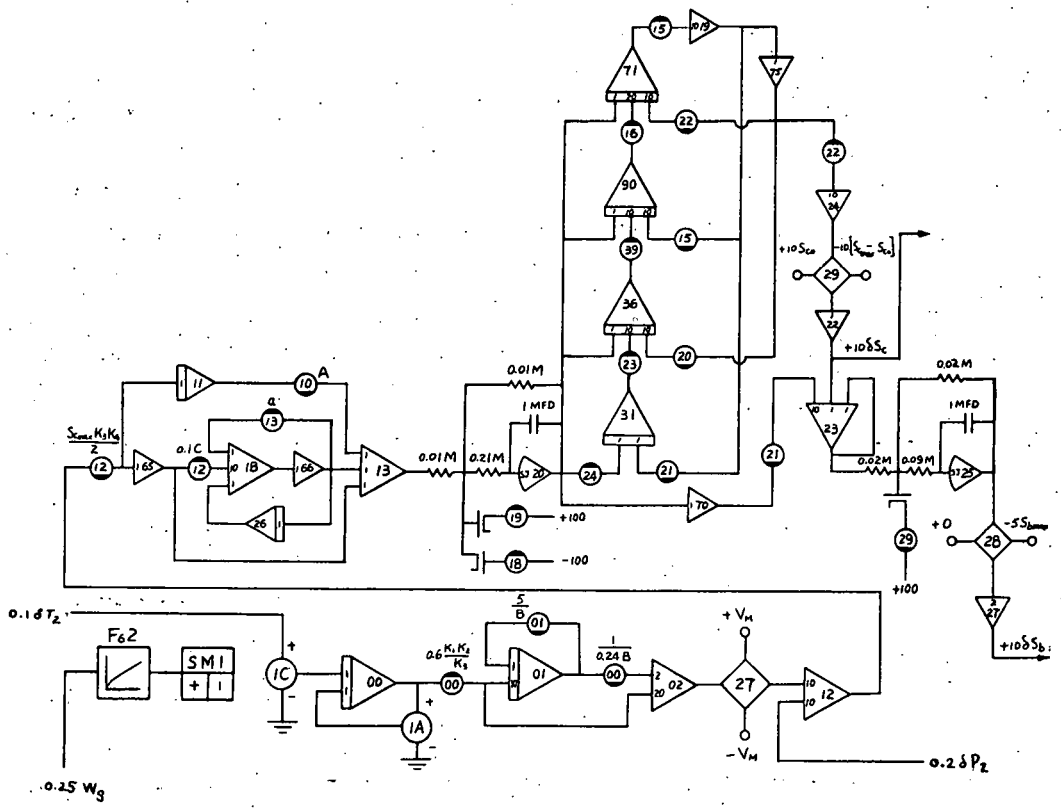

Figure 15.13 Computer diagram for control system.

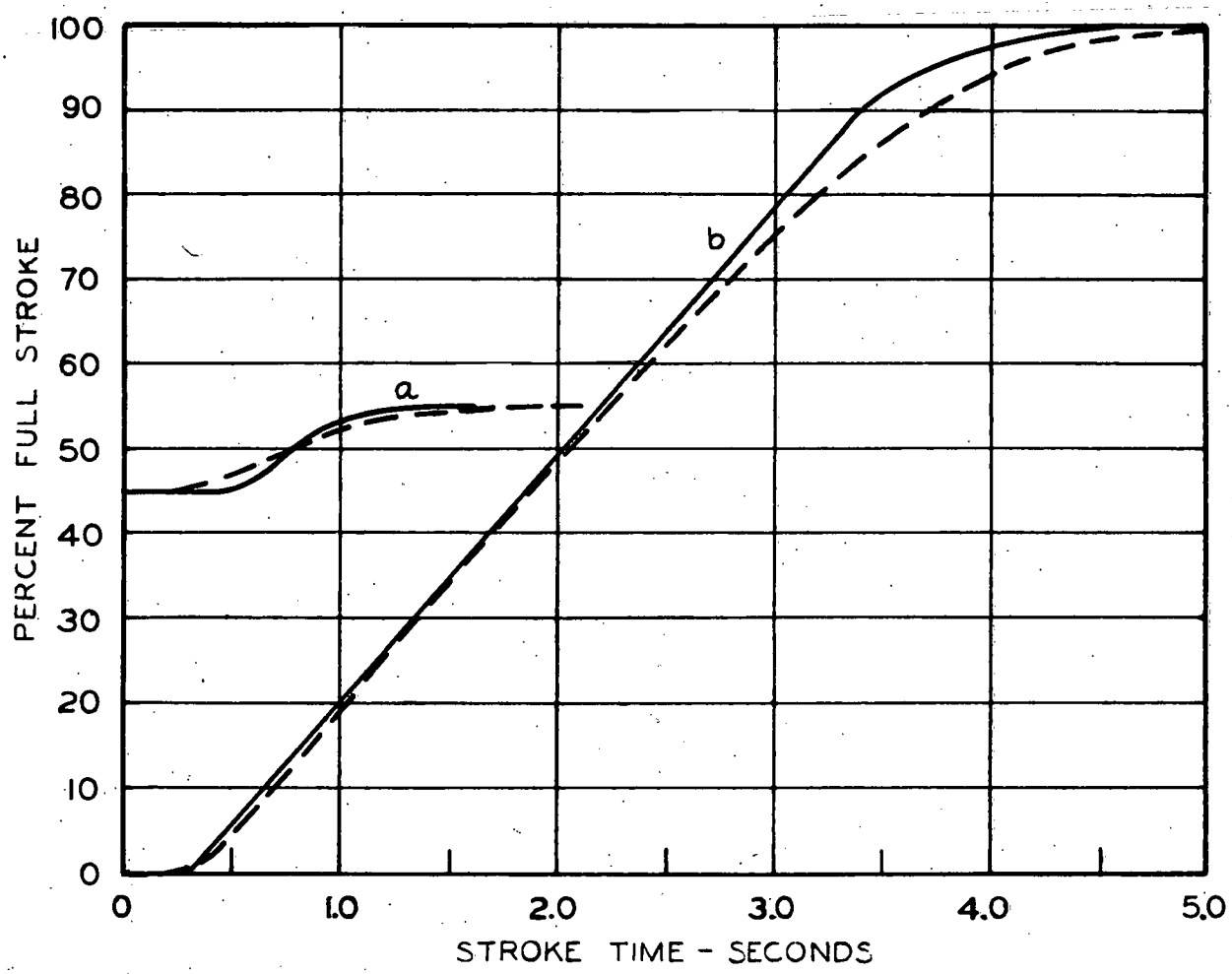

Figure 15.14 Step response of inlet valve actuator. Code: a) response to 10 per cent step; b) response to 100 per cent step. Measured curve is solid; simulated curve is dashed. (A-C Dwg. 43-024-801)

15.13 Simulation of the Feedwater System

Figure 15.15 is the computer circuit for the feedwater flow equation shown below

$$\delta W_{fw} = \frac{\delta W_s}{1 + \tau_{fv} s} \tag{15.36}$$

Figure 15.16 is the computer circuit for the feedwater enthalpy equations, a relay is used for the nonlinear change.

$$\delta h_{fw} = \frac{\partial h_{fw}}{\partial W_s} \frac{\delta W_s}{1 + \tau_{fh} s}, \quad \delta W_s \geq -19\% W_{so}$$

$$\delta h_{fw} = -5.4\% h_{fwo}, \quad \delta W_s \leq -19\% W_{so} \tag{15.37}$$

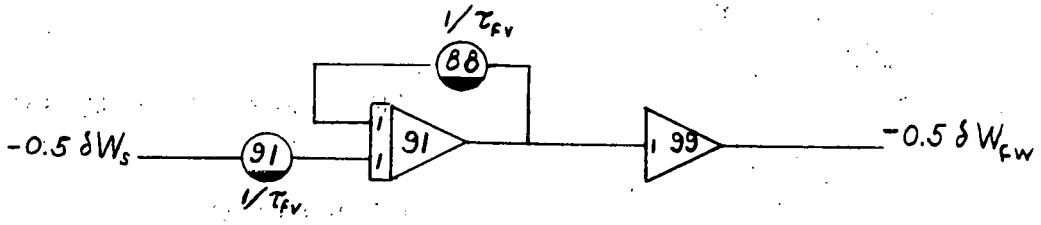

Figure 15.15 Computer diagram for feedwater flow.

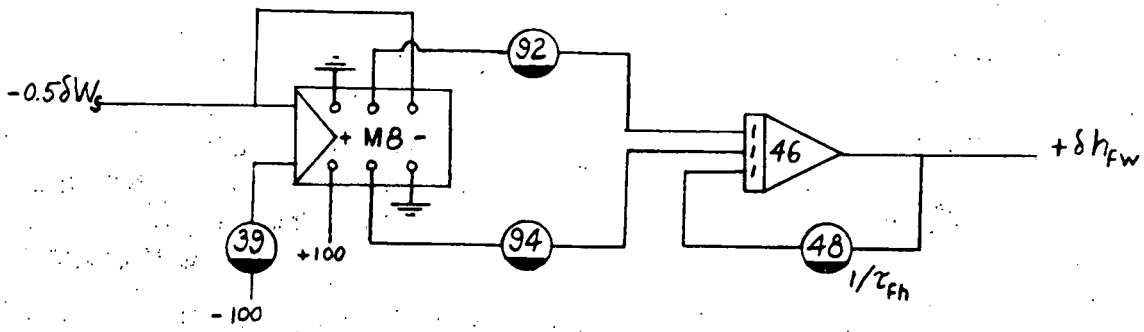

Figure 15.16 Computer diagram for feedwater enthalpy.

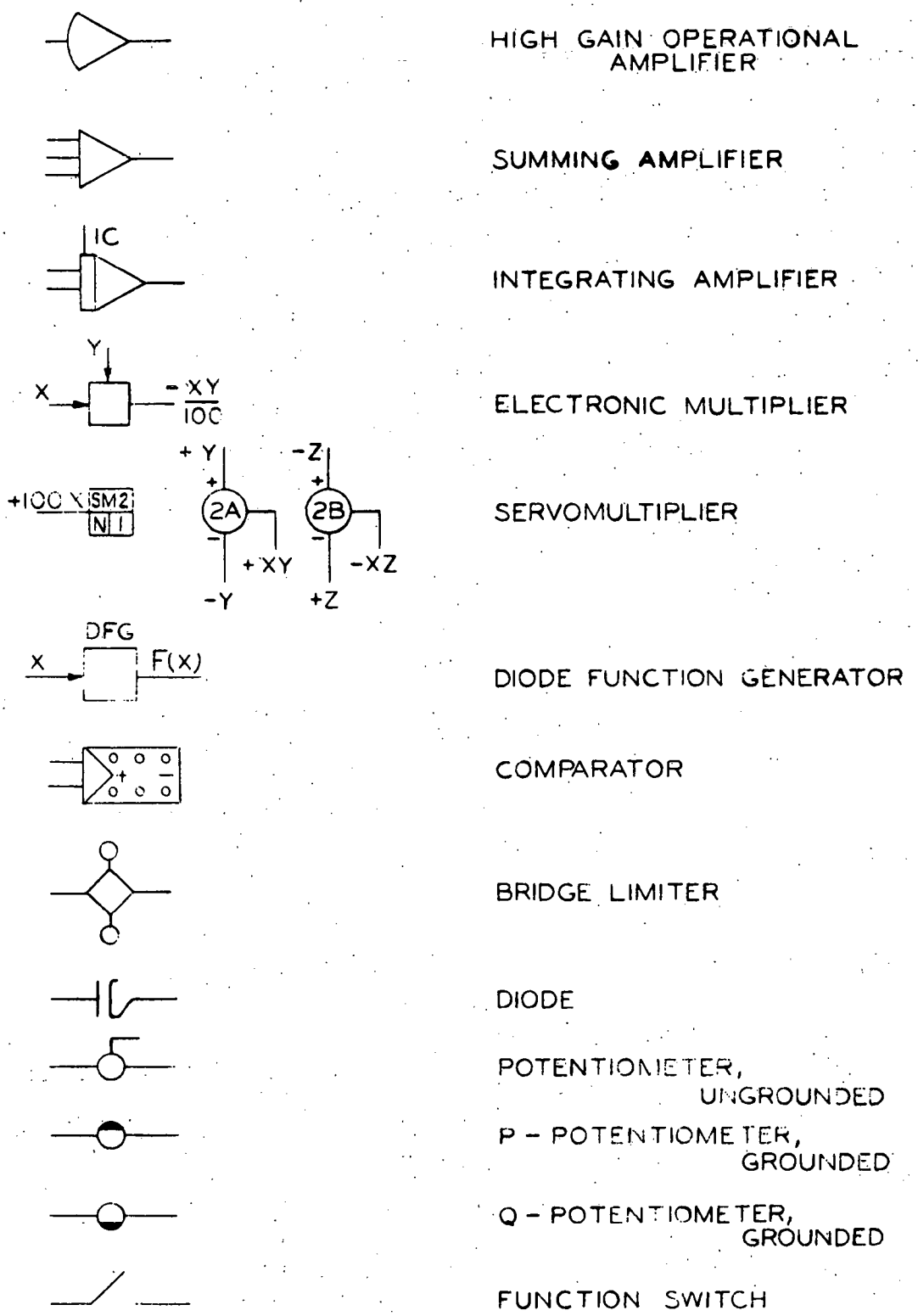

Figure 15.17 Computer diagram symbols. (A-C Dwg. 43-024-806)

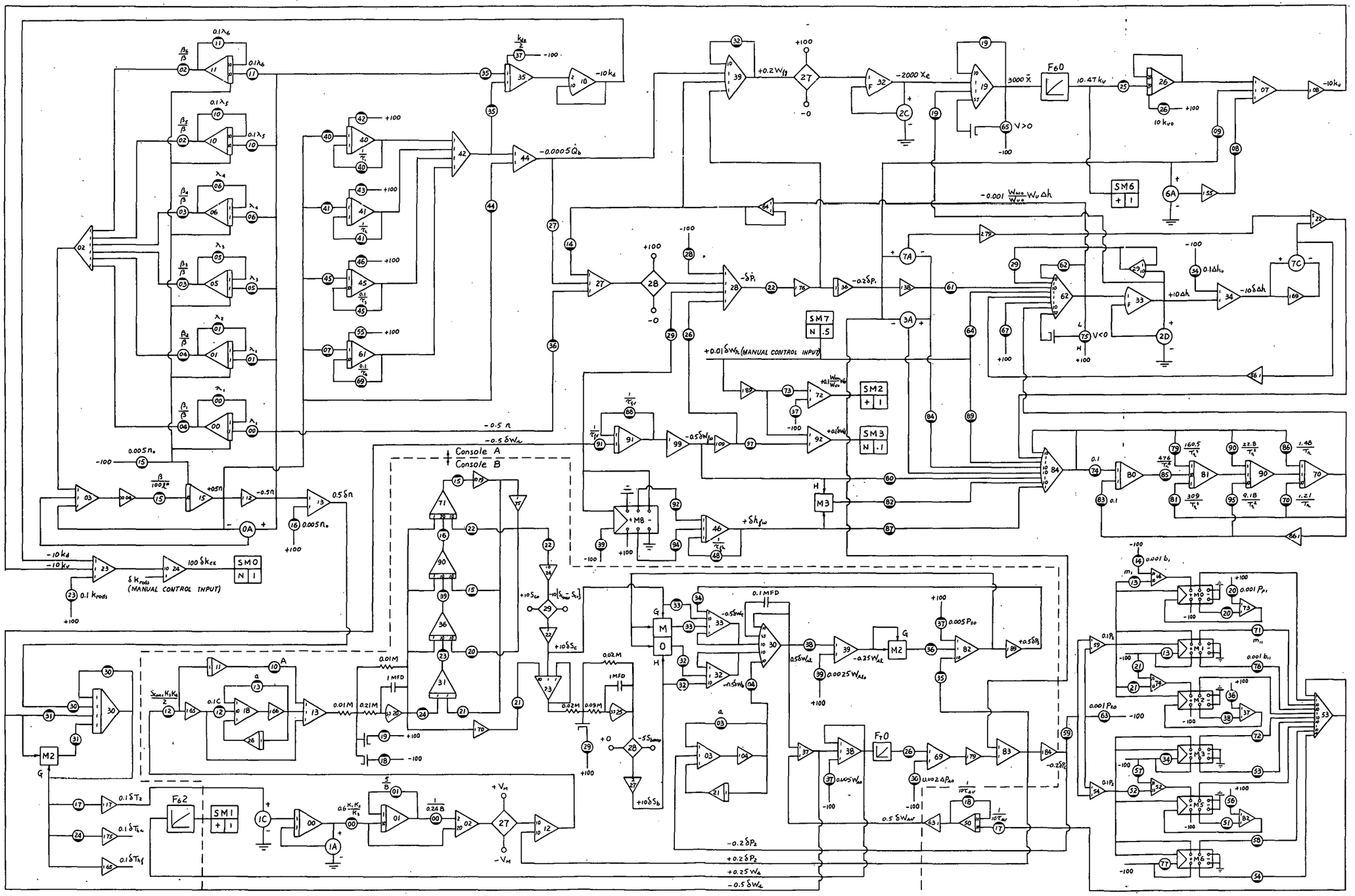

Figure 15.18 Computer diagram of Pathfinder transient simulator.

APPENDIX A

POTENTIOMETER SETTINGS

PATHFINDER SIMULATOR CONSOLE A, Q POT

Q POT	SYSTEM	PARAMETER	SETTING
00	Neutron Kinetics	λ_1	0.0127
01	Neutron Kinetics	λ_2	.0317
02	Neutron Kinetics	β_5/β .	.1280
03	Neutron Kinetics	β_4/β	.4068
04	Neutron Kinetics	β_2/β	.2130
05	Neutron Kinetics	λ_3	.1150
06	Neutron Kinetics	λ_4	.3110
07	Boiler Fuel Element	$10^{-3} \times \frac{F_4}{\bar{\tau}_4} \times \frac{\dot{Q}_{go}}{n_o}$	.7450
08	Pressure effects on reactivity	$\frac{5\times10^3}{10.47}(1-\bar{\alpha})\left[\frac{1}{v_g}\frac{\partial v_g}{\partial P} - \frac{1}{h_{fg}}\frac{\partial h_{fg}}{\partial P} - \frac{1}{v_f}\frac{\partial v_f}{\partial P}\right]$	.5158
09	Pressure effects on react.	$50\ \frac{\partial k_v}{\partial \bar{\alpha}} \times (1-\bar{\alpha})\frac{1}{v_f}\frac{\partial v_f}{\partial P}$	.1280
10	Neutron Kinetics	$0.1\ \lambda_5$	.1400
11	Neutron Kinetics	$0.1\ \lambda_6$	.3870
12			
13	Safety Valve #1	$P_{pi}/1000$	.6080
14	Vessel Pressure	$W_{vo}/DW_{wo}\ 5\times10^{-3}$	.2785
15	Neutron Kinetics	$0.005\ n_o$	.5000
16	Time Axis	1 volt/sec.	.0100
17	Superheater	$H_h'\ (h_{20} - h_{10})/Cp_2\ \dot{Q}_{ho}$	.3480
18			
19	Void React.	$200\ E/h_{fg}\ I$	.1920
20	Safety Valve #1	$P_{P1}/1000$	.6080
21	Safety Valve #2	$b_2/1000$	.1862
22	Vessel Pressure	Scaling factor	.2000
23	React. Sum.	$0.1(k_{do} + k_{vo})$	.7100
24	Superheater	$H_h'\ (h_{ho} - h_{10})/cp\ \dot{Q}_{ho}$	.7300
25			
26	Vessel Pressure	$2\ v_f\ h_{fg}/D\ v_{fg}$	.0050
27			
28			
29	Subcooling	$.001\ W_{Po}$	.0111

PATHFINDER SIMULATOR CONSOLE A, Q POT (Cont.)

Q POT	SYSTEM	PARAMETER	SETTING
30	Superheater	$0.2\ \dot{Q}_{ho}/C_h\ n_o$	0.7795
31	Superheater	$100\ H_h'/0.5\ W_{so}\ C_h$	.5339
32	Void React.	$2.5 \times 10^{-5}\ h_{fg}$	.1816
33			
34	Subcooling	$0.1\ \Delta h_o$	.3790
35	Doppler React.	$100\ \frac{\dot{Q}_{go}}{n_o}\ \frac{\partial K_d}{\partial T_{avg}}\ \frac{1}{C}\ (1-\gamma)$	.2150
36	Safety Valve #2	$P_{P2}/1000$	.6150
37	Subcooling	$10^{-4}\ W_{wo}$	.6285
38			
39	Feedwater	$0.5\ (1.9 \times 10^{-3}\ W_{so})$	.1620
40	Boiler Fuel Element	$1/\tau_1$	.1471
41	Boiler Fuel Element	$1/\tau_2$	.7874
42			
43			
44	Boiler Fuel Element	$10^{-3} \times \gamma \times \frac{\dot{Q}_{go}}{n_o}$ $\gamma = 3\%$	.0447
45	Boiler Fuel Element	$10^{-3} \times \frac{F_3}{\tau_3} \times \frac{\dot{Q}_{go}}{n_o}$	.1461
46			
47			
48	Feedwater	$1/\tau_{fh}$	.0500
49			
50			
51	Safety Valve #3	$P_{P3} - P_{R3}/1000$	.0480
52	Safety Valve #3	m_3	.3767
53	Safety Valve #2	$b_{22}/1000$	.1828
54	Safety Valve #3	$b_{33}/1000$	.1822
55	Boiler Fuel Element	$10^{-5}\ \frac{F_4\ \dot{Q}_{go}}{2}$	.0596
56	Safety Valve #3	$P_{P3}/1000$	.6200
57	Safety Valve #3	$b_3/1000$	.1856
58	Safety Valve #3	m_{33}	.2938
59			
60			
61	Subcooling	$10^{-5}\ W_{ro} \left(1 - \frac{1}{\rho J \partial h_f/\partial P}\right)$	.6870

PATHFINDER SIMULATOR CONSOLE A, Q POT (Cont.)

Q POT	SYSTEM	PARAMETER	SETTING
62	Subcooling	$0.1 \frac{W_{ro}}{W_{wo}}$	0.1112
63			
64	Subcooling	$0.1\ \Delta h_o$	.3790
65	Voids Reactivity	Adjusted to make output ($\bar{x}$) always > 0	.005
66			
67	Subcooling	$10^{-5}\ W_{ro}\ \Delta h_o$	.2653
68			
69	Boiler Fuel Element	$0.1 \frac{1}{\tau_4}$	.6250
70	Subcooling	$1.21/T_r$	.1624
71	Safety Valve #1	m_{11}	.2841
72	Safety Valve #2	m_{22}	.2973
73	Subcooling	W_{wo}/W_{ro}	.8993
74	Subcooling	Scaling Factor	.1000
75			
76	Safety Valve #1	$b_{11}/1000$	.1727
77	Safety Valve #3	$P_{P3}/1000$	.6200
78			
79	Subcooling	$160.5/T_r^3$	.3890
80	Subcooling	$.002\ (h_{fo} - h_{fwo})$	.2922
81	Subcooling	$309/T_r^3$	.7480
82	Subcooling	Scaling Factor	.0200
83	Subcooling	Scaling Factor	.1000
84	Subcooling	$10^{-4}\left[W_{ro}\left(1 - \frac{1}{\rho J \partial h_f/\partial P}\right) - W_{fwo}\right]$	.6688
85	Subcooling	$476/T_r^4$	.1545
86	Subcooling	$1.48/T_r$	.1988
87	Subcooling	$.001\ W_{fwo}$	.1800
88	Feedwater System	$1/\tau_{fv}$	.5000
89	Subcooling	$0.1\ \Delta h_o$	.3790
90	Subcooling	$22.8/T_r^2$	.4110
91	Feedwater System	$1/\tau_{fv}$	.5000
92	Feedwater System	$2 \frac{\partial h_{fw}/\partial W_s}{\tau_{fh}}$	.0540
93			
94	Feedwater System	$5.4 \times 10^{-4}\ h_{fwo}/\tau_{fh}$	.0088
95	Subcooling	$9.18/T_r^2$	.1653
96			
97	Subcooling	Scaling Factor	.0200

PATHFINDER SIMULATOR CONSOLE A, P POT

P POT	SYSTEM	PARAMETER	SETTING
00	Neutron Kinetics	λ_1	0.0127
01	Neutron Kinetics	λ_2	.0317
02	Neutron Kinetics	β_6/β	.0260
03	Neutron Kinetics	β_3/β	.1880
04	Neutron Kinetics	β_1/β	.0380
05	Neutron Kinetics	λ_3	.1150
06	Neutron Kinetics	λ_4	.3110
07			
08			
09			
10	Neutron Kinetics	$0.1 \times \lambda_5$	.1400
11	Neutron Kinetics	$0.1 \times \lambda_6$	.3870
12			
13	Safety Valve #1	m_1	.3700
14	Safety Valve #1	$b_1/1000$	.1781
15	Neutron Kinetics	$0.01\ \beta/l^*$	.7778
16	Neutron Kinetics	$5 \times 10^{-3}\ n_o$	.5000
17			
18	Subcooling	Sealing Factor	.2000
19	Void React.	$0.067/I$	.1241
20	Safety Valve #1	$P_{P1} - P_{R1}/1000$	.0470
21	Safety Valve #2	m_2	.3800
22			
23			
24			
25	Void React.	$0.05\ \partial k_v/\partial\bar{\alpha}$	.9550
26	Void Redistribution	$10\ k_{vo}$	.6020
27	Vessel Pressure	$1/D \times 5 \times 10^{-4}$	.2500
28	Vessel Pressure	$h_{fg}\ W_{so}/100D$	.1574
29	Vessel Pressure	$\frac{2(1 + V_{fo}/V_{fgo})h_{fgo}}{D}$	.1868
30	Superheater	H_h'/C_h	.4568
31	Superheater	$0.2 \left[\frac{T_{hfo} - T_{hso} + (h_{ho}-h_1/c_p)}{C_h\ W_{s_o}}\right] H_h'$	.4547
32			
33			
34	Safety Valve #2	$P_{P2}/1000$	.6150

PATHFINDER SIMULATOR CONSOLE A, P POT (Cont.)

P POT	SYSTEM	PARAMETER	SETTING
35	Doppler React.	$\frac{\partial k_d}{\partial T_{avg}} \frac{1}{C} \times 10^5$	0.1490
36	Vessel Pressure	$2 \frac{\dot{Q}_{mo}}{n_o D}$	.0065
37	Doppler React.	$k_{do}/2$	.5400
38	Safety Valve #2	$P_{P2} - P_{R2}/1000$	.0480
39			
40	Boiler Fuel Element	$10^{-3} \frac{F_1}{\tau_1} \times \frac{\dot{Q}_{go}}{n_o}$	.1554
41	Boiler Fuel Element	$10^{-3} \frac{F_2}{\tau_2} \times \frac{\dot{Q}_{go}}{n_o}$	.1525
42	Boiler Fuel Element	$10^{-5} \frac{F_1 \dot{Q}_{go}}{2}$	.5285
43	Boiler Fuel Element	$10^{-5} \frac{F_2 \dot{Q}_{go}}{2}$	.0969
44			
45	Boiler Fuel Element	$0.1 \frac{1}{\tau_3}$	.1961
46	Boiler Fuel Element	$10^{-5} \frac{F_3 \dot{Q}_{go}}{2}$	.0373
47			
48			
49			
50			

PATHFINDER SIMULATOR CONSOLE B, Q POT

Q POT	SYSTEM	PARAMETER	SETTING
00	Control	1/0.24 B	0.4167
01	Control	5/B	.5000
02			
03	Steam System	Arbitrary constant that must be near 1.0 for differentiation.	.80
04	Steam System	$2.5 \times 144 \frac{V_s}{k R_s T_{20}}$ (Where T_{20} is $^{\circ}R$)	.875
05			
06			
07			
08			
09			
10	Control	0.1 A	.0250
11			
12	Control	$S_{c\ max} K_3 K_4/2$	.0400
13			
14	Control	$.05 S_{co}$	.4220
15	Control	$0.1 \frac{91.8}{22.8}$ (Scaling)	.403
16			
17			
18			
19			
20	Control	$0.1 \frac{309}{160.5}$	.193
21	Control	Scaling	.5000
22	Control	$0.1 \frac{12.1}{1.48}$ (Scaling)	.8160
23			
24			
25			
26	Steam System	$20 \frac{\Delta P_{so}}{W_{so}^{1.62}}$	.2900
27			
28			
29	Control	Adjusted such that the maximum rate of change of S_b is 9.44/0.4 S_b/sec.	.1462
30			
31			
32	Steam System	$100/5\sqrt{P_3 v_s}$	.7500

PATHFINDER SIMULATOR CONSOLE B, Q POT (Cont.)

Q POT	SYSTEM	PARAMETER	SETTING
33	Steam System	$100/5\sqrt{P_{3}v_{s}}$	0.7500
34	Steam System	$S_{co}/0.5\sqrt{P_{3}v_{s}}$	.6330
35			
36	Steam System	$.002\ \Delta P_{so}$	.1300
37	Steam System	$.005\ W_{so}$	.8550
38	Steam System	Scaling Factor	.5000
39	Steam System	$.0025\ W_{slo}$	.4275
40			

PATHFINDER SIMULATOR CONSOLE B, P POT

P POT	SYSTEM	PARAMETER	SETTING
00	Control	$0.6 \frac{K_1 K_2}{K_3}$	0.1200
01			
02			
03			
04			
05			
06			
07			
08			
09			
10			
11			
12	Control	0.1 R	.1000
13	Control	$0 < (1 - P13) \ll P12$ (Differentiating approximation)	.9000
14			
15	Control	$0.1 \frac{1.48}{\tau_a}$	.1644
16	Control	$0.05 \frac{22.8}{1.48\ \tau_a}$	.8550
17			
18	Control	Adjusted such that the maximum rate of change of S_b is 9.44/3.0 S_b/sec.	.0028
19	Control'		
20			
21			
22	Control	Scaling Factor	.8000
23	Control	$0.2 \frac{476}{160.5\ \tau_a}$	.6590
24	Control	Scaling Factor	.5000
25			
26			
27			
28			
29			
30			
31			
32	Steam System	$P_{30}/100\sqrt{P_{30} v_s}$	.2025

PATHFINDER SIMULATOR CONSOLE B, P POT (Cont.)

P POT	SYSTEM	PARAMETER	SETTING
33	Steam System	$P_{30}/100\sqrt{P_{30}v_s}$	.2025
34			
35	Steam System	Scaling Factor	.2500
36	Steam System	$\frac{\Delta P_{slo}}{W_{slo}^2} \times \frac{50}{0.0625}$	.2735
37	Steam System	$\frac{\Delta P_{slo}}{200}$	.0500
38			
39	Control	$0.1 \frac{160.5}{22.8 T_a}$	.7825
40			

APPENDIX B

SYMBOLS

For all variables, the subscript "o" denotes steady-state, rated value, and the prefix "δ" denotes departure from this value.

ENGLISH		RATED VALUES
A	Reset setting on unit RP-1.0a (See Figure 12.1)	0.25 sec^{-1}
B	Rate setting prop + rate unit (See Figure 12.1)	10 sec.
b_i, b_{ii}	Safety valve flow characteristic intercepts on Figure 11.3	lb/sec.
C	Total boiler fuel heat capacity	1300 Btu/F
C_h	Superheater fuel heat capacity per ft^2 at hot spot	0.0985 Btu/ft^2-F
C_i	Concentration of i^{th} group delayed neutron precursors	
c_p	Specific heat of steam at superheater hot spot	0.54 Btu/lb-F
c_{p2}	Specific heat of steam at superheater exit	0.555 Btu/lb-F
D	Denominator of Eq. 5.6	8000 Btu/psi
E	Graphically evaluated subcooling effect (Eq. 7.4)	0.375
F_i	Gain of i^{th} term in boiler fuel transfer function (See Eq. 3.19 for values)	
H_h	Heat Transfer coefficient at surface of superheater hot spot.	0.167 Btu/sec-F-ft^2
H_h'	$H_{ho}/1 + \frac{H_{ho}(h_{ho}-h_{10})}{c_p \dot{Q}_{ho}}$	0.0450 Btu/sec-F-ft^2
h_1	Enthalpy of steam at superheater inlet	1203.1 Btu/lb
h_2	Enthalpy of steam at superheater exit	1368.0 Btu/lb
h_f	Enthalpy of saturated water at 615 psia	475.1 Btu/lb
h_g	Enthalpy of saturated steam at 615 psia	1203.1 Btu/lb
h_{fg}	$h_g - h_f$	728.0 Btu/lb
h_{in}	Enthalpy of water entering core	471.5 Btu/lb
h_{fw}	Enthalpy of feedwater entering vessel	328.7 Btu/lb
h_{ps}	Enthalpy of pump seal in-flow	60.1 Btu/lb
h_r	Enthalpy of water just down-stream of feed-water inlet	471.3 Btu/lb
h_h	Enthalpy of steam at superheater hot spot	1539.6 Btu/lb
Δh	$h_f - h_{in}$	3.6 Btu/lb
$\mathcal{I}$	$\int_o^1 \varphi_1'(Z)\, \dot{Q}(Z)\, dZ$ (See Section 7)	0.537
J	Energy Conversion factor	5.4 ft^3-lb/Btu-in^2
k	Ratio of specific heats of superheated steam	1.285
k_{ex}	Excess reactivity	0 Dollars
k_d	Reactivity decrease (Doppler effect) due to fuel temperature rise above 489 F	1.08 Dollars

ENGLISH		RATED VALUES
k_v	Reactivity decrease due to core void formation	5.92 Dollars
k_{rods}	Reactivity due to control rod position	7.0 Dollars
K_1	Sensitivity of T_2 transducer (See Figure 12.1)	$K_1K_2 = \frac{0.2 \times 50 \text{ volts}}{800 \text{ F}}$
K_2	Gain of prop + rate unit (See Figure 12.1)	
K_3	Sensitivity of P_2 transducer (See Figure 12.1)	50 volts/800 psi
K_4	Gain of unit RP-10a (See Figure 12.1)	0.14
l^*	Effective neutron lifetime	9×10^{-5} sec.
m_i; m_{ii}	Safety valve flow characteristic slopes on Figure 11.3	lb/sec-psi
N	Biot number for heat transfer from boiler fuel pellets	32.8
n	Total neutron population in units of percent	100%
P_1	Reactor dome pressure	615 psia
P_2	Superheater exit pressure	555 psia
P_3	Turbine inlet pressure	541 psia
P_{pi}	Popping pressure of i^{th} safety valve (See Figure 11.3)	psia
P_{ri}	Reset pressure of i^{th} safety valve (See Figure 11.3)	psia
ΔP_s	Superheater pressure drop	60 psi
ΔP_{sl}	Steam line pressure drop	11 psi
$\dot{Q}_b$	Power transferred to water in boiler fuel boxes	1.49×10^5 Btu/sec
$\dot{Q}_h$	Heat flux generated at superheater hot spot	38.4 Btu/sec-ft^2
$\dot{Q}_m$	Remaining power transferred to water outside boiler fuel boxes	2.6×10^3 Btu/sec
$\dot{Q}_p$	Pump energy delivered to water	697 Btu/sec
$\dot{Q}(z_o)$	Fraction of boiler power delivered to subcooled water	0.15
q_h	Heat flux delivered to steam at superheater hot spot (including unbonding effect)	38.4 Btu/sec-ft^2
R	Rate setting on unit RP-10a (See Figure 12.1)	10 sec.
R_s	Gas constant for superheater steam	81.5 ft/F
s	Laplace operator (d/dt)	sec^{-1}
S_b	Dump valve capacity coefficient	0.0 in-ft$^{3/2}$/sec.
S_c	Turbine inlet valve capacity coefficient	8.44 in-ft$^{3/2}$/sec.
t	Time	sec.
T	Boiler fuel characteristic time (See Eq. 3.6)	36.3 sec.
T_2	Superheater steam outlet temperature	725 F
T_{hf}	Superheater fuel hot spot temperature	1270 F
T_{hs}	Superheater steam temperature at hot spot	1040 F
T_r	Transport time through subcooled water	7 sec.

ENGLISH		RATED VALUES
V_s	Volume of main steam line	308 ft^3
v_f	Specific volume of saturated water	0.0201 ft^3/lb
v_g	Specific volume of saturated steam	0.753 ft^3/lb
v_{fg}	$v_g - v_f$	0.732 ft^3/lb
v_s	Specific volume of superheated steam	1.20 ft^3/lb
W_b	Steam flow through bypass valve	0 lb/sec.
W_d	Water flow through downcomer	7.079 lbs/sec.
W_{fg}	Steam flow at core exit	171.1 lbs/sec.
W_{fw}	Feedwater flow rate	180.1 lbs/sec.
W_p	Water flow to purification system	11.1 lbs/sec.
W_{ps}	Pump seal water in-flow	2.1 lbs/sec.
W_r	Flow at pump discharge	7,260 lbs/sec.
W_s	Steam flow through superheater	171.1 lbs/sec.
W_{sl}	Steam flow through steam line	171.1 lbs/sec.
W_{sv}	Total steam flow through safety valves	0.0 lbs/sec.
W_t	Steam flow through turbine inlet	171.1 lbs/sec.
W_v	Recirculation flow entering vessel	7,250 lbs/sec.
W_w	Recirculation flow entering boiler fuel boxes (proportional to W_v)	6,480 lbs/sec.
$\bar{x}$	Mean effective boiler steam fraction by weight	0.0123
x_e	Steam fraction at boiler core exit by weight	0.0264

GREEK		RATED VALUES
$\bar{\alpha}$	Mean effective boiler steam fraction by volume	0.308
β	Total delayed neutron fraction	0.007
β_i	Delayed neutron fraction of i^{th} group (See Table below)	

Parameters of Delayed Neutron Groups

i	β_i/β	λ_i
1	0.0380	0.0127
2	0.2130	0.0317
3	0.1880	0.1150
4	0.4068	0.3110
5	0.1280	0.1400
6	0.0260	0.3870

γ	Fraction of power transferred immediately to boiler channels by gamma radiation	0.03
λ_i	Decay constant of i^{th} delay group (See Table above)	

SYMBOLS (Cont.)

GREEK		RATED VALUES
ρ	Density of subcooled water in vessel	49.5 lbs/ft^3
$\bar{\tau}_4$	Average time constant of 4th to ∞^{th} partial fractions in boiler fuel transfer function expansion	0.16 sec.
τ_a	Response time of pneumatic inlet valve actuator	0.9 sec.
τ_{fh}	Time constant by which feedwater temperature lags steam flow	20 sec.
τ_{fv}	Time constant by which feedwater flow lags steam flow	2 sec.
τ_i	Time constant of i^{th} term in boiler fuel transfer function (See Eq. 3.19 for values)	sec.
τ_{sv}	Opening time lag of safety valves	0.1 sec.
τ_v	Time constant of void redistribution	0.05 sec.

PARTIAL DERIVATIVES	VALUES
$\partial h_f/\partial P$	0.2 Btu/lb-psi
$\partial h_g/\partial P$	-0.017 Btu/lb-psi
$\partial h_{fg}/\partial P$	-0.217 Btu/lb-psi
$\partial h_{fw}/\partial W_s$	0.54 Btu-sec/lb^2
$\partial k_d/\partial T_{avg}$	1.9×10^{-3} Dollars/F
$\partial K_v/\partial \bar{\alpha}$	19.2 Dollars
$\partial v_f/\partial P$	3.75×10^{-6} ft^3/lb-psi
$\partial v_g/\partial P$	-1.25×10^{-3} ft^3/lb-psi
$\partial W_{fg}/\partial \dot{P}_1$	-0.57 lbs/psi